

Colloquium: Anomalous statistics of laser-cooled atoms in dissipative optical lattices

Gadi Afek

Quantum Art, Ltd., Nes-Ziona 7414003, Israel

Nir Davidson

Department of Physics of Complex Systems, Weizmann Institute of Science, Rehovot 76100, Israel

David A. Kessler  and Eli Barkai

Department of Physics, Institute of Nanotechnology and Advanced Materials, Bar-Ilan University, Ramat-Gan 52900, Israel

 (published 27 September 2023)

Diffusion occurs in numerous physical systems throughout nature, drawing its generality from the universality of the central limit theorem. Approximately a century ago it was realized that an extension to this type of dynamics can be obtained in the form of “anomalous” diffusion, where distributions are allowed to have heavy power-law tails. Owing to a unique feature of its momentum-dependent dissipative friction force, laser-cooled atomic ensembles can be used as a test bed for such dynamics. The interplay between laser cooling and anomalous dynamics bears deep predictive implications for fundamental concepts in both equilibrium and nonequilibrium statistical physics. The high degree of control available in cold-atom experiments allows for the parameters of the friction to be tuned, revealing transitions in the dynamical properties of the system. Rare events in both the momentum and spatial distributions are described by non-normalized states using tools adapted from infinite ergodic theory. This leads to new experimental and theoretical results that illuminate the various features of the system.

DOI: [10.1103/RevModPhys.95.031003](https://doi.org/10.1103/RevModPhys.95.031003)

CONTENTS

I. Introduction	1
II. Lévy Dynamics and Sisyphus Cooling	3
A. Lévy versus Gauss central limit theorem, Lévy flights, and Lévy walks	3
B. The basics of Sisyphus cooling	4
III. Anomalous Statistics and Infinite Densities	6
A. Momentum space	6
B. Position space	10
C. Position-momentum correlations	13
IV. Implications for Fundamental Concepts in Statistical Physics	14
A. Scaling Green-Kubo relation	14
B. Breakdown of ergodicity	16
C. Violation of the equipartition theorem	16
V. Lévy Statistics and Power Laws in Other Atomic Systems	17
A. Motional broadening in two-level system ensembles with a heavy-tailed frequency distribution	17
B. Lévy dynamics in subrecoil laser cooling	18
VI. Discussion and Summary	18
Acknowledgments	19
References	20

I. INTRODUCTION

Diffusive processes such as Brownian motion are ubiquitous in nature. In these the position coordinates of an ensemble

of noninteracting particles, all starting from a common origin, are normally distributed. This is a manifestation of the central limit theorem as the basic motion is composed of many random, uncorrelated steps. Mathematically Brownian motion can be described either using a stochastic differential equation that models the trajectory of a single particle (Gardiner, 1985; Van Kampen, 2007) or with the diffusion equation relating to the description of the entire ensemble. The asymptotic time dependence of the mean-squared displacement of such a motion is characteristically given by $\langle x^2 \rangle \sim t$, where $\langle \dots \rangle$ denotes an average over the ensemble.

It is now well established (Bouchaud and Georges, 1990; Metzler and Klafter, 2000; Sokolov and Klafter, 2005) that this is merely a particular case of a much richer set of phenomena where the dynamics differs in general from the “normal” behavior, and $\langle x^2 \rangle \sim t^\beta$, where the exponent β is not necessarily unity. Studying the mathematical properties of an extension to the standard central limit theorem, Lévy (1937) considered the problem of the summation of a large number of independent and identically distributed random variables whose variance diverges (Sec. II.A). This arises when the distribution of the random variables is heavy tailed and decays as a sufficiently small power law. The resulting family of distributions describing the sum are called stable distributions, giving rise to the normal Gaussian as a special (albeit important) case. Early physical manifestations of these include canonical work on spectroscopy (Holtmark,

1919) and the study of the distribution of gravitational forces acting on a tracer (Chandrasekhar, 1943). These statistical laws are now widely used tools in many fields, such as econophysics (Mantegna and Stanley, 1999), soft matter and biophysics (Shusterman *et al.*, 2004; Song *et al.*, 2018), dynamics of blinking quantum dots (Stefani, Hoogenboom, and Barkai, 2009), and hydrodynamics (Kelly and Meerschaert, 2019).

One simple model allowing access to the full richness of the anomalous diffusion parameter space is a generalization of the Lévy flight (Mandelbrot, 1982; Shlesinger, Zaslavsky, and Frisch, 1995). In this random-walk model, a walker “jumps” a certain distance and then dwells at the arrived location for a certain time. Jump distances and dwell times are random variables, both drawn from distributions that can in general be heavy tailed or can have diverging moments (Scher and Montroll, 1975). Intuitively it can be understood that if the dwell time distribution has a heavy tail the dynamics can become “subdiffusive” ($\beta < 1$), whereas if the moments of the jump distances are allowed to diverge the dynamics may become “superdiffusive” ($\beta > 1$). An important issue when dealing with such power-law distributions is that jumps can occur on many widely different scales. Since in physical processes long jumps are expected to take longer than short ones and since a truly diverging jump length can never realistically be obtained, a modification to the original Lévy approach was put forth. In the simplest version of this “Lévy walk” model (Shlesinger, West, and Klafter, 1987; Zaburdaev, Denisov, and Klafter, 2015), a fixed finite speed is prescribed, ensuring that long jumps take longer than short ones. More generally a power-law correlation between the distance covered in a jump and the time duration of the jump was considered (Shlesinger, West, and Klafter, 1987). Other generalizations of the Lévy walk have also been proposed and analyzed as models of anomalous diffusion (Albers and Radons, 2018; Bothe, Sagues, and Sokolov, 2019; Vezzani, Barkai, and Burioni, 2020).

While much is known about the stochastic foundation of the Lévy walk and its applications, a physical model that allows control over the transition between the phases of the dynamics could pave the way to deeper understanding. As originally described by Marksteiner, Ellinger, and Zoller (1996), laser-cooled atoms (in certain parts of parameter space) are ideal for this purpose. This realization gave rise to a series of questions regarding fundamental issues in statistical physics, such as the non-Maxwellian nature of the velocity distribution, rare events in heavy-tailed processes, calculation of anomalous transport constants, and the ergodic properties of these nonequilibrium processes (Bardou *et al.*, 2002; Lutz and Renzoni, 2013). As a concrete example of such a fundamental concept, consider the two-time velocity autocorrelation function $\langle v(t_2)v(t_1) \rangle$. For Brownian motion and a vast number of other transport systems, this quantity is stationary and depends only on the time difference $|t_2 - t_1|$. This has many consequences, for example, for the calculation of the diffusion constant using the Einstein-Green-Kubo approach and also for the ergodic properties of the system. Under certain conditions, however, this stationarity property does not hold for laser-cooled atoms, and instead the correlations exhibit scale invariance where the

ratio of the two times becomes important. This leads to new ideas on transport and ergodicity.

Laser cooling is a well-established experimental technique for obtaining extremely low temperatures of atomic ensembles.¹ A momentum-dependent friction force is generated by external optical fields, reducing the atoms’ momentum toward zero. The canonical example is that of Doppler cooling (Hänsch and Schawlow, 1975; Wineland and Dehmelt, 1975; Wineland, Drullinger, and Walls, 1978; Phillips, 1998), where pairs of counterpropagating beams, detuned from the relevant two-level atomic resonance, selectively reduce the momentum of fast-moving atoms. The associated minimal Doppler temperature T_D , brought about by the balance between the friction and random emissions of photons jolting the atoms, is given by $k_B T_D = \hbar\Gamma/2$, where Γ is the natural linewidth of the excited state, k_B is the Boltzmann constant, and \hbar is the reduced Planck constant. This was originally thought to be a fundamental limit for the ability to laser cool atomic systems, and it therefore was a surprise when temperatures below the Doppler limit were obtained experimentally (Chu, 1998; Cohen-Tannoudji, 1998) via a process later called Sisyphus cooling (Sec. II.B). The key to explaining this discovery was the multilevel, degenerate nature of realistic atoms. The random momentum recoils $\hbar k$ due to scattered photons give rise to a second lower bound for the temperature, the recoil limit $k_B T_R/2 = \hbar^2 k^2/2M = E_R$, where E_R is the recoil energy, M is the atomic mass, and k is the wave number. Temperatures even lower than the recoil limit have been achieved through other techniques such as subrecoil laser cooling (Aspect *et al.*, 1988; Bardou *et al.*, 1994), Raman and Raman-sideband cooling (Kasevich and Chu, 1992; Vuletić *et al.*, 1998), and evaporative cooling (Anderson *et al.*, 1995) relying on different physical mechanisms.

For Sisyphus cooling, the particular dependence of the friction force on the atomic momentum leads to anomalous kinetics. The phase-space trajectory of an atom in the semiclassical approximation of the laser-cooling mechanism has been analyzed theoretically with tools from quantum optics and the theory of stochastic processes (Dalibard and Cohen-Tannoudji, 1989; Marksteiner, Ellinger, and Zoller, 1996).

While anomalous dynamics can be found in many systems within the context of ultracold atomic physics (Niedenzu, Grießer, and Ritsch, 2011; Meir *et al.*, 2016; Kindermann *et al.*, 2017; Zheng and Cooper, 2018; Dechant *et al.*, 2019), in this Colloquium we focus on recent developments in both the theoretical and the experimental understanding of the anomalous dynamics of atoms undergoing Sisyphus cooling. The model presented departs from the standard descriptions of Lévy walks, which are usually postulated *ad hoc*, and lays bare the mechanism behind the non-normal kinetics. From an experimental perspective, the model allows unique control of the basic phenomenon enabling the transition between

¹The temperature of standard gases is given by the width of the stationary Gaussian momentum distribution. In the context of this work, however, momentum distributions typically deviate from Gaussianity, and hence the definition is more subtle. This definition is discussed at the end of Sec. III.A.

different phases of the dynamics. This is in stark contrast to most superdiffusive systems, say, in the atmosphere or in the context of cell biology, where there is little experimental control over the basic features of the process. The main point of view is to present the modifications of the basic Lévy walk model that emerge and the consequences for basic concepts of equilibrium and nonequilibrium physics hand in hand with relevant experimental results. Among the topics discussed are the power-law distributions in momentum and position as well as their correlations (Sec. III) and the implications of fundamental concepts in statistical physics such as the Einstein-Green-Kubo relation, the breakdown of ergodicity and energy equipartition, and the relation to infinite ergodic theory (Sec. IV).

II. LÉVY DYNAMICS AND SISYPHUS COOLING

A. Lévy versus Gauss central limit theorem, Lévy flights, and Lévy walks

The process of Brownian motion was modeled by Einstein, Smoluchowski, and others (Kubo, 1957; Hnggi and Marchesoni, 2005; Majumdar, 2007). It is natural that the underlying random walk describing it is a Gaussian process, as this is precisely what the central limit theorem predicts for a process where the total displacement at long times is a sum of many independent random displacements. Deviations from normal, Gaussian, Brownian motion can be parametrized using the random walk governed by Lévy laws.

Central limit theorems deal with the problem of summation of a large number N of independent, identically distributed random variables $\{\chi_i\}$. The sum $S = \sum_{i=1}^N \chi_i / N^{1/\mu}$ scaled by some power $1/\mu$ of N is considered. The probability density function (PDF) of S is given by the inverse Fourier transform of its characteristic function,

$$\begin{aligned} \langle \exp(ikS) \rangle &= \left\langle \exp\left(\frac{ik\chi_1}{N^{1/\mu}}\right) \right\rangle \cdots \left\langle \exp\left(\frac{ik\chi_N}{N^{1/\mu}}\right) \right\rangle \\ &= \left\langle \exp\left(\frac{ik\chi}{N^{1/\mu}}\right) \right\rangle^N, \end{aligned} \quad (1)$$

where on the left the average is taken over the random variable S and on the right it is taken with respect to the random variable χ . The result is a direct outcome of the assumption that the random variables $\{\chi_i\}$ are independent and identically distributed, so the expectation value factorizes. We assume here that the PDF of χ is symmetric so that its mean is zero. Two examples are the Gaussian PDF $P_G(\chi) = \exp(-\chi^2/2\sigma^2)/\sqrt{2\pi\sigma^2}$ with a standard deviation σ and a Lorentzian PDF $P_L(\chi) = [\pi(1 + \chi^2)]^{-1}$. The first is an example of a distribution with finite moments, while the second has a power-law tail, and its variance diverges. The characteristic functions of the Gaussian and Lorentzian are $\tilde{P}_G(k) = \exp(-k^2\sigma^2/2)$ and $\tilde{P}_L(k) = \exp(-|k|)$, respectively. Related to the divergence of the variance, the characteristic function of the Lorentzian exhibits nonanalytical behavior at $k = 0$, $P_L(k) \sim 1 - |k|$ and the second derivative with respect to k at this point diverges. More generally if $P(\chi) \sim |\chi|^{-(1+\nu)}$ for large $|\chi|$ and $0 < \nu < 2$, then for small k we have

$\tilde{P}(k) \sim 1 - A|k|^\nu$, where A is a scale parameter used as an input for the theory (Bouchaud and Georges, 1990). For $\nu < 2$ the variance of the summand diverges. On the other hand, for any parent distribution of χ with a finite variance, we have $P(k) \sim 1 - \sigma^2 k^2/2$, where the leading term reflects the fact that $P(\chi)$ is normalized. Using Eq. (1), two generic possibilities are then found in the limit of $N \rightarrow \infty$. If the variance of $P(\chi)$ is finite,

$$\langle \exp(ikS) \rangle \rightarrow \left(1 - \frac{\sigma^2 k^2}{2N}\right)^N = \exp(-\sigma^2 k^2/2), \quad (2)$$

where we choose $\mu = 2$ and use the definition of the exponential limit. This implies a diffusive scaling for the sum. It also means that the PDF of the scaled sum S is Gaussian for any parent distribution with a finite variance σ . In contrast, if $P(\chi)$ exhibits power-law decay with $\nu < 2$, then μ is chosen² such that $\mu = \nu$, and

$$\langle \exp(ikS) \rangle \rightarrow \left(1 - \frac{A|k|^\nu}{N}\right)^N = \exp(-A|k|^\nu). \quad (3)$$

In this case superdiffusive scaling emerges, as the sum of the random variables grows as $N^{1/\nu}$.

To summarize, the sum of random variables is scaled with $N^{1/\mu}$. Equation (2) implies that if the variance is finite, then $\mu = 2$, while Eq. (3) together with the definition of the exponential function results in $\mu = \nu$ if $\nu < 2$ (and the variance diverges). The inverse Fourier transform of Eq. (3) is the PDF of the sum S and is also the well-known symmetric stable density or Lévy density (Bouchaud and Georges, 1990; Amir, 2020),

$$L_{\nu,0}(S) = \frac{1}{2\pi} \int_{-\infty}^{\infty} dk \exp(ikS - |k|^\nu), \quad (4)$$

where the subscript 0 indicates symmetric functions and the width scale A is set to unity. In particular, the case $\nu = 1$ is the Lorentzian, and $\nu = 2$ is the Gaussian.

Two forms of central limit theorems now emerge: the first is usually associated with Gauss³ [Eq. (2)], and the second is associated with Lévy [Eq. (3)]. When a system exhibits power-law statistics of the Lévy type, the largest summand in the set $\{\chi_i\}$ is of the order of the entire sum (Chistyakov, 1964; Vezzani, Barkai, and Burioni, 2019). The fact that the variance diverges implies that the underlying random walk is a fractal, also called a self-similar object. This is easily visualized considering a 2D Lévy flight, as depicted in Fig. 1.

Specific examples of Lévy stable densities had already emerged in physics, absent the general mathematical framework, in the context of the summation of a large number of forces or energies more than a century ago. In his line-shape

²Though a rigorous proof of the central limit theorem is beyond the scope of this Colloquium, note that any other choice of $\nu \neq \mu$ would not give a meaningful limit when $N \rightarrow \infty$.

³Though in modern physics this is called a Gaussian (which dates back to 1809), its roots precede Gauss and extend well into the 18th century with Bernoulli, de-Moivre, and Laplace (Stigler, 1986).

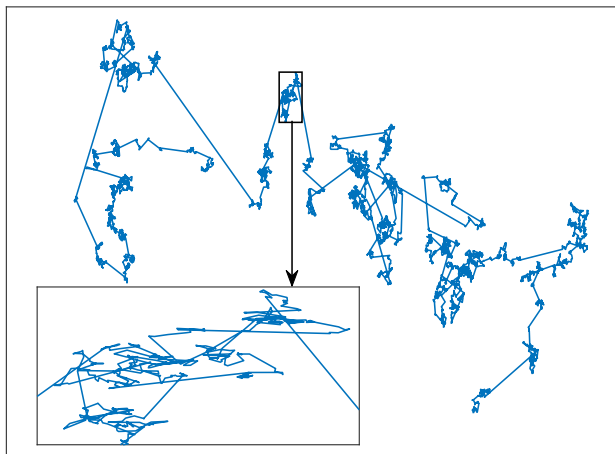


FIG. 1. Lévy flights are random-walk processes where the jump distances are obtained from heavy-tailed power-law distributions with infinite variance [Eq. (3)]. Depicted is an example of a two-dimensional flight, with the horizontal and vertical axes representing spatial dimensions and a Lévy index $\nu = 1.4$. The direction of a given jump is rotated from that of the previous one by a random angle uniformly distributed between 0 and 2π . Inset: depiction of the fractal, self-similar nature of the dynamics, which is similarly characterized by a small number of long flights and a large number of short ones.

theory, [Holtmark \(1919\)](#) considered the distribution of the sum of many perturbations acting on an ion. A similar problem was later discussed by [Chandrasekhar \(1943\)](#) in an astrophysical context. The Holtmark distribution is a particular yet significant case of the Lévy stable distribution, with $\nu = d/n$, where $d = 3$ is the dimension of the system and $n = 2$ is the power of the spatial dependence of the interaction potential, i.e., gravitational or Coulomb. It applies when considering the force projected on one of the axes and when the bath particles are uniformly distributed in space. In his work on the energy transfer due to multiple scatterings in ionization, [Landau \(1944\)](#) constructed what would become known as the one-sided Lévy stable distribution. Similar ideas and behaviors were found for single molecules in low temperature glasses ([Barkai, Silbey, and Zumofen, 2000](#); [Barkai *et al.*, 2003](#)) and in models of active dynamics ([Kanazawa *et al.*, 2020](#)).

The notion of a Lévy flight, where jump displacements are drawn from a common PDF with a power-law tail and summed, is problematic for a process describing spatial dynamics, as larger jump distances in space are expected to take longer. The power-law tail of the jump-size distribution means that the mean-squared displacement (MSD) of the Lévy flight is infinite, which is unphysical, as any real system will have a maximal speed of propagation. To remedy this, the concept of Lévy walks was introduced by [Shlesinger, West, and Klafter \(1987\)](#) and [Zaburdaev, Denisov, and Klafter \(2015\)](#).

The simplest (one-dimensional) version of the Lévy walk considers a particle starting at the origin at $t = 0$. A random-walk-duration τ is drawn from a heavy-tailed PDF $\psi(\tau)$. A random velocity is also drawn, for example, $\pm V_0$, each with probability 1/2. During this interval the motion is ballistic,

reaching $x = \pm V_0\tau$. The process is then repeated (“renewed”) and a new pair of walk duration and velocity is drawn. The position $x(t)$ of the particle is limited by the ballistic light cone $-V_0t < x(t) < V_0t$, and the moments of $x(t)$ never diverge for any finite t . If the distribution of walk durations does not have power-law tails but is exponential, this model is essentially the Drude model for transport of electrons in metals, and the diffusion is normal. In the Lévy walk case, the walk-duration PDF is heavy tailed, $\psi(\tau) \sim \tau^{-(1+\eta)}$. Here if $1 < \eta < 2$ the variance of the flight duration diverges, while if $0 < \eta < 1$ the mean flight duration also diverges. This yields three dynamical phases for the MSD ([Zaburdaev, Denisov, and Klafter, 2015](#)),

$$\langle x^2(t) \rangle \sim \begin{cases} t^2, & 0 < \eta < 1, \\ t^{3-\eta}, & 1 < \eta < 2, \\ t, & \eta > 2. \end{cases} \quad (5)$$

When $\eta < 1$ the dynamics are ballistic, whereas for $1 < \eta < 2$ the spreading is superdiffusive. When the first two moments of the PDF of the jump duration are finite ($\eta > 2$), normal diffusion is recovered. In the Lévy walk, therefore, a natural cutoff is created by introducing the finite velocity, curing the unphysical divergence of the variance of displacement in the corresponding Lévy flight. Another major difference between Lévy walks and Lévy flights is that in the latter the number of steps N is fixed, as in any other random-walk process, whereas in the Lévy walk the number of renewals in the time interval $(0, t)$ is itself a random variable ([Godreche and Luck, 2001](#)).

There are many physical applications of Lévy walks. For example, blinking quantum dots ([Brokmann *et al.*, 2003](#); [Margolin and Barkai, 2005](#); [Stefani, Hoogenboom, and Barkai, 2009](#)) work in the ballistic phase $0 < \eta < 1$, where the “effective velocity” is the intensity of emitted light that jumps between dark and bright states with power-law-distributed sojourn times. The position of the random walker corresponds to the total number of photon counts that exhibits superdiffusive statistics, as seen in experiments ([Margolin *et al.*, 2006](#)). Lévy walks also appear in the motion of bacterial colonies ([Ariel *et al.*, 2015](#)) and in many other systems ([Zaburdaev, Denisov, and Klafter, 2015](#)).

B. The basics of Sisyphus cooling

The mechanism by which anomalous diffusion is manifested within the context of cold atomic ensembles in dissipative optical lattices⁴ is related to the nonlinear nature of the momentum-dependent optical friction force $f(p)$ acting on the atoms ([Dalibard and Cohen-Tannoudji, 1989](#); [Castin and Molmer, 1990](#); [Agarwal and Molmer, 1993](#); [Marksteiner, Ellinger, and Zoller, 1996](#)). In the semiclassical approximation and for a given set of damping strength \mathcal{A} and momentum capture range p_c , it takes the form ([Castin, Dalibard, and Cohen-Tannoudji, 1991](#))

⁴Not all atomic species trapped in near-resonant optical lattices display such behavior. Bosonic Yb, for example, lacks the appropriate level structure and has no Sisyphus effect ([Kostylev *et al.*, 2014](#)).

$$f(p) = -\frac{Ap}{1 + (p/p_c)^2}. \quad (6)$$

A and p_c are functions of the experimental parameters of the system. A slow atom with $|p|/p_c \ll 1$ will experience a draglike force $f \sim -p$ similar to the Stokes friction acting on a Brownian particle in fluid, whereas a fast atom instead feels a weak force $f \sim -1/p$. Intuitively, fast-moving atoms tend to remain fast, leading to large flights in space and in turn to anomalous Lévy-type motion.

To realize this friction (Chu, 1998; Cohen-Tannoudji, 1998; Foot, 2005), consider the qualitative picture of an atom that has a lower energy level with angular momentum $J = 1/2$ and an upper energy level with $J' = 3/2$ that moves through a standing wave formed by two counterpropagating laser beams with orthogonal linear polarizations (Fig. 2, top panel). The resulting polarization depends on the relative phase of the two laser beams and varies periodically with position x , changing from linear at, say, $x = 0$, to σ^- at $x = \lambda/8$ to orthogonal linear at $x = 2\lambda/8$ to σ^+ at $x = 3\lambda/8$. λ , of the order of a few hundreds of nanometers, is the wavelength of the lattice lasers. This polarization lattice causes periodic modulation of the states in the lower level manifold due to Stark shifts, enhancing the probability of the downhill transitions when the atom is at the top of the potential (and hence the term *Sisyphus* from Greek mythology). The result is a net cooling effect as the atom, on average, slows down. The energy drops in Fig. 2 (bottom panel) correspond to the absorption-emission events shown in the top panel. They are depicted as uneven to reflect the fact that the process is probabilistic and does not necessarily occur exactly at the peak.

Sisyphus cooling reaches a nonequilibrium steady state where the friction force that biases the system toward zero momentum is balanced with the fluctuations caused by spontaneous emission. For “deep” lattices, where the potential modulation depth U_0 defined in Fig. 2 is large, the temperature is proportional to and of the order of U_0 (Cohen-Tannoudji, 1998). This can be intuitively understood given that once the energy of the atom is smaller than U_0 it cannot climb up the hill, and hence at this stage cooling is ineffective (Fig. 2, bottom panel). As U_0 is reduced, the temperature reaches a minimum at some U_0^{\min} and then rises sharply upon further reduction of U_0 (“shallow” lattices). At this minimum, to which typical experimental systems are tuned, $\langle E_k \rangle \sim U_0^{\min}$.

Sisyphus cooling was extensively studied experimentally for a variety of atomic species. Typically pairs of counterpropagation red-detuned laser beams are used to generate the dissipative lattice, although three or four beams at proper angles can also be used (Kerman et al., 2000), depending on the dimensionality of the problem. The lattice depth is controlled via the power and detuning of the cooling lasers, and magnetic fields must be kept below a few tens of milligauss to suppress shifts of the Zeeman levels that might hinder the Sisyphus effect. Finally, additional lasers are needed to “repump” the atoms into the cycling transition levels, but their direct effect on the atomic motion is usually negligible. In the deep-lattice regime, the temperature can be determined by measuring the standard deviation of the velocity distribution, a task performed mostly using the

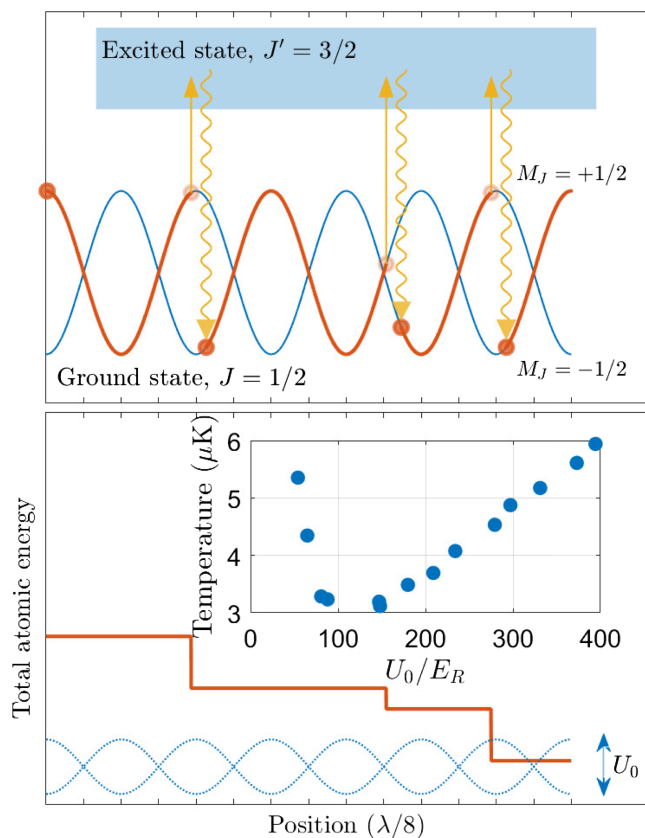


FIG. 2. Lévy dynamics can arise in the motion of atoms undergoing Sisyphus cooling. Top panel: two counterpropagating, orthogonally linearly polarized laser beams generate a periodic spatial modulation of the polarization. The atomic ground state energy sublevels $M_J = +1/2$ and $-1/2$ are then perturbed by the standing light wave such that the atom travels up and down hills of potential energy. When the laser frequency is tuned below the atomic resonance frequency, state-changing photon scattering is more probable around the top of the potential hills, where the spontaneously emitted photon has a higher frequency than the absorbed one, illustrated as wiggly and straight yellow lines, respectively. Bottom panel: as a result an atom, moving from left to right in the depicted example along the thicker orange line, loses energy on average due to photon scattering, so cooling becomes efficient. The main control parameter is the modulation depth of the lattice U_0 . Inset: measurement of the temperature of Sisyphus-cooled ^{133}Cs atoms as the lattice depth is varied (Jersblad, Ellmann, and Kastberg, 2000), demonstrating a sharp increase of temperature when U_0/E_R decreases. Adapted from Castin, Dalibard, and Cohen-Tannoudji, 1991.

time-of-flight technique, where a cloud of atoms is released from all confining fields and is allowed to freely expand. This generates a mapping of the atomic velocity distribution onto its spatial distribution after the expansion (assuming sufficient time elapses for the cloud to expand to a size much larger than its original width). The density profile of the expanded atoms, now describing their initial velocity distribution, is then imaged using fluorescence or absorption imaging. Additional techniques to measure atomic velocity distributions are based on velocity-selective Raman transitions (Moler et al.,

1992), on spatial correlation functions (Saubaméa *et al.*, 1997), or on measuring the survival probability after a sudden decrease of the trap depth [applicable for single atoms (Alt *et al.*, 2003; Tuchendler *et al.*, 2008)].

The inset of Fig. 2 shows the result of such a time-of-flight temperature measurement after three-dimensional Sisyphus cooling of ^{133}Cs atoms (Jersblad, Ellmann, and Kastberg, 2000) as a function of the optical lattice depth U_0 . The results show a minimal temperature at $U_0^{\text{min}}/E_R \approx 100$. The distinction between shallow ($U_0 < U_0^{\text{min}}$) versus deep lattices ($U_0 > U_0^{\text{min}}$), which will be shown to mark the transition between different regimes in the dynamics, then naturally follows.

III. ANOMALOUS STATISTICS AND INFINITE DENSITIES

A. Momentum space

We now turn to a quantitative description of the anomalous dynamics of the momentum distribution for 1D motion in the dissipative lattice after averaging over the lattice period and using the semiclassical approximation. Generally this is valid in the shallow-lattice regime and ignores trapping in the wells of the optical lattice. More specifically it requires the following: (i) The laser must be weak, meaning that the saturation parameter $s_0 \ll 1$ [s_0 is a measure of the occupation of the excited state proportional to the laser intensity (Foot, 2005)]. (ii) The atomic kinetic energy must be large compared to the lattice depth such that all positions along the lattice are considered equiprobable allowing spatial averaging. (iii) The atomic momentum change $\Delta p \gg \hbar k$, where k is the wave number of the laser field (Lutz, 2003). The validity of the semiclassical approximation has been tested using full quantum Monte Carlo wave function simulations (Castin, Dalibard, and Cohen-Tannoudji, 1991; Marksteiner, Ellinger, and Zoller, 1996), and it has been shown to quantitatively hold under the previously described conditions, assuming an ideal atomic level structure of $J = 1/2 \rightarrow J' = 3/2$. For other level structures the results show a qualitative agreement.

This semiclassical treatment is a useful approximation since the long jumps giving rise to the Lévy diffusion are not influenced by the trapping potential. The procedure of the derivation of the Fokker-Planck equation involves a spatial averaging over the wells, namely, it is assumed that spatial modulation of the optical lattice has a marginal effect on the anomalous statistics (Castin, Dalibard, and Cohen-Tannoudji, 1991; Marksteiner, Ellinger, and Zoller, 1996). In the opposite limit of deep lattices, the spatial structure of the lattice and the energy surfaces play an important role and cannot simply be averaged out.

It has been shown (Castin, Dalibard, and Cohen-Tannoudji, 1991; Hodapp *et al.*, 1995; Lutz, 2004) that the dynamics of the momentum PDF $W(p, t)$ is governed by the following Fokker-Planck equation⁵:

⁵A first derivation of the Fokker-Planck equation for atoms in a field of laser radiation pressure was given by Letokhov and Minogin (1981). Equation (7) is derived in the semiclassical limit using an expansion of the master equation in terms of the recoil velocity.

$$\frac{\partial W}{\partial t} = -\frac{\partial}{\partial p}[f(p)W] + \frac{\partial}{\partial p}\left[D(p)\frac{\partial W}{\partial p}\right], \quad (7)$$

which is valid for shallow lattices. The diffusive term $D(p) = D_0 + D_1/[1 + (p/p_c)^2]$ describes stochastic fluctuations of the momentum where D_0 and D_1 are functions of the experimental parameters (Castin and Molmer, 1990; Marksteiner, Ellinger, and Zoller, 1996). Unlike the friction force that vanishes in the limit of large momentum, the momentum diffusion becomes p independent in this limit and $D(p) \rightarrow D_0$. The simple relation between friction and dissipation, in the spirit of the Einstein relation, is hence invalid.

The steady-state solution $W(p)$ of Eq. (7) was derived by Lutz (2003). Using the force given by Eq. (6) and the previously discussed diffusive term, it reads

$$W(p) \sim \left[1 + \frac{D_0}{D_0 + D_1} \left(\frac{p}{p_c}\right)^2\right]^{-\tilde{U}_0/2}. \quad (8)$$

The width of the momentum distribution is determined by p_c , and it has a power-law tail with an exponent expressed in terms of \tilde{U}_0 as $W(p) \sim |p|^{-\tilde{U}_0}$. Emerging from the Fokker-Planck equation as an important dimensionless parameter in the system, \tilde{U}_0 is defined in terms of the experimental parameters as

$$\tilde{U}_0 = \mathcal{A} \frac{p_c^2}{D_0} = \frac{1}{C} \frac{M\delta s_0}{\hbar k^2} = \frac{1}{C} \frac{U_0}{E_R}. \quad (9)$$

In Eq. (9) δ is the detuning of the laser from the atomic transition frequency. Different values are cited in the literature for the proportionality constant C , reflecting the complexity of experimental atomic systems beyond the simplified models (Castin and Molmer, 1990; Marksteiner, Ellinger, and Zoller, 1996). The exact numerical value does not, however, have a profound effect on the results presented here, and therefore it is reasonable to treat C as a dimensionless fitting parameter. Even though both the detuning of the laser from the atomic resonance and its intensity affect the potential depth as well as the photon scattering rate, the effective temperature and indeed the anomalous dynamics depend only on the single parameter \tilde{U}_0 .

The second moment of the steady-state momentum $\langle p^2 \rangle$, usually considered a measure of the temperature, diverges when $\tilde{U}_0 < 3$. Moreover, when $\tilde{U}_0 < 1$ the solution itself is no longer normalizable and there is no steady state at all. The first experimental verification of Eq. (8) was presented by Douglas, Bergamini, and Renzoni (2006), where an ensemble of ^{133}Cs atoms was exposed to a 3D Sisyphus lattice of variable depth.⁶ The atomic momentum distribution, measured by time of flight, is presented in Fig. 3. The results, representing an average over 200 separate images where extra care was taken to balance the radiation-pressure force from the counterpropagating beam pairs, led Douglas, Bergamini, and

⁶Although Eq. (8) is derived for 1D cases, in isotropic cases it can also apply to higher dimensions (Lutz, 2003).

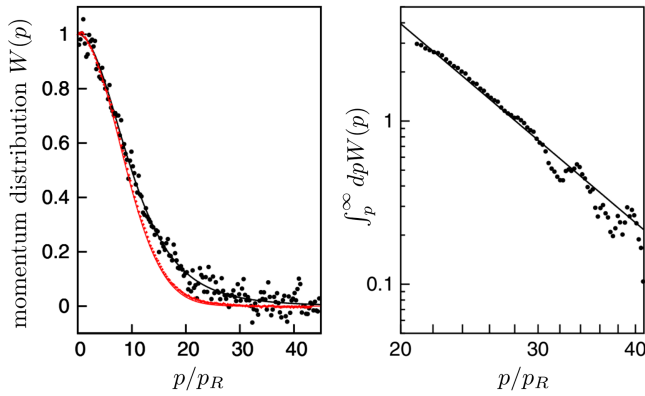


FIG. 3. Analysis of the atomic dynamics under the unique Sisyphus friction [Eq. (6)] predicts a non-Gaussian steady state in momentum [Eq. (8)]. Left panel: results of a time-of-flight measurement of the momentum distribution $W(p)$ of an ensemble of ^{133}Cs atoms as a function of their momentum, rescaled by the recoil momentum $p_R = \sqrt{2ME_R}$. A deep lattice (small red markers, almost coinciding with the thin red line) is compared with a shallow lattice (large black circles). The solid lines represent fits by Eq. (8), giving a Gaussian distribution for the deep lattice (thin red line) and a power law for the shallow lattice (thick black line). Right panel: integrated data from the left panel describing the probability of the momentum being larger than some value p . Plotted on a log-log scale, it reveals the power-law nature of the distribution. Adapted from Douglas, Bergamini, and Renzoni, 2006.

Renzoni (2006) to conclude that they represent a statistically significant indication of the power-law tails of the momentum distribution. This can be seen in the right panel of Fig. 3, where the probability of an atom having a momentum larger than some value p is shown to fit a power law over two decades. The non-Gaussianity of the momentum distribution of atoms in the deep-lattice regime was studied experimentally by Jersblad et al. (2004) using ^{133}Cs . They fitted time-of-flight data to several test functions, including the power-law-type distribution of Eq. (8) and a double Gaussian, and concluded that a double Gaussian provides a better fit to the experimental data. Bimodal distributions were also found by Dion et al. (2016).

In analyzing the dynamics described in Eq. (7), it is convenient to also consider the corresponding Langevin equation representing the phase-space trajectory of a single particle. There is a standard procedure for obtaining the corresponding Langevin equation from a given Fokker-Planck equation (Van Kampen, 2007), wherein the drift term corresponds to an external force and the diffusion term arises from the external noise. The analysis of trajectories is extremely useful for a myriad of reasons, ranging from the ease of simulations that allow insight into the nature of individual trajectories to more subtle properties of the system such as the analysis of time averages to tackle issues like ergodicity (discussed in Sec. IV). For simplicity we set $D_1 = 0$, since it modifies neither the asymptotic $|p| \rightarrow \infty$ behavior of the diffusive term nor the cooling force, and therefore does not affect the main conclusions. Transforming to dimensionless time $t \rightarrow At$, momentum $p \rightarrow p/p_c$, and

position $x \rightarrow xMA/p_c$, the Langevin equation, with $\xi(t)$ the white Gaussian noise with zero mean and second moment $\langle \xi(t)\xi(t') \rangle = \delta(t-t')$, reads (Barkai, Aghion, and Kessler, 2014)

$$\frac{dp}{dt} = f(p) + \sqrt{\frac{2}{\tilde{U}_0}} \xi(t), \quad \frac{dx}{dt} = p, \quad (10)$$

where the dimensionless form of the force of Eq. (6) is $f(p) = -p/(1+p^2)$.

The non-normalizability of the steady state for $\tilde{U}_0 < 1$ points to a dynamical transition. The time it takes a particle with momentum $p > 0$ to cross $p = 0$ is random and the PDF of these times is described by a power law $\psi(\tau) \sim \tau^{-(1+\eta)}$, with $0 < \eta \leq 1$ for $\tilde{U}_0 \leq 1$ (Marksteiner, Ellinger, and Zoller, 1996; Barkai, Aghion, and Kessler, 2014). The non-normalized steady state is thus related to the divergence of the mean return time of the momentum. Even though the energy cannot realistically diverge, measurements of the ensemble-averaged kinetic energy $\langle p^2 \rangle / 2M$ do exhibit a sharp transition at a certain \tilde{U}_0 below which the energy increases dramatically (Fig. 2, inset). The divergence of the return time and the vanishing of the normalization of the steady state are generic themes that often appear together in other systems (Aghion, Kessler, and Barkai, 2019).

A theoretical challenge now arises. Assuming that the Fokker-Planck equation is valid, is the associated steady state $W(p)$ a valid description over times that are long but finite? It turns out that the steady state by itself does not yield a complete description of the momentum distribution. In particular, all moments of the momentum distribution as specified by the time-dependent Fokker-Planck equation are finite for any finite measurement time, in contrast to the steady-state prediction based on Eq. (8). To obtain these moments, including the second moment (which as noted gives the ensemble-averaged kinetic energy) for $\tilde{U}_0 < 3$, a new tool is needed, called the infinite covariant density.

Infinite covariant density.—It has been shown that the time-independent solution is not an adequate description of the system, as it gives rise to infinite moments. The full time-dependent solution gives physically meaningful answers for all finite times; however, its exact form is not analytically attainable. A useful approximate result can be obtained if the problem is broken in two, with the regimes $p \ll \sqrt{t}$ and $p \sim \sqrt{t}$ focused on separately. In the former case, the equilibrium answer is a good approximation. In the latter case, however, a new type of approximation is obtained that amounts to a non-normalizable density. Such a seemingly paradoxical mathematical object has been given the name infinite density and will be shown to be a crucial tool for correctly generating the second and higher moments of the momentum distribution.

The dimensionless form of the steady-state momentum distribution corresponding to Eq. (8) is

$$W(p) = \mathcal{N}(1+p^2)^{-\tilde{U}_0/2} \quad \text{for } \tilde{U}_0 > 1, \quad (11)$$

with $\mathcal{N} = \Gamma(\tilde{U}_0/2) / \sqrt{\pi} \Gamma[(\tilde{U}_0-1)/2]$. This describes the steady state of the process defined in Eq. (10), with $\Gamma(x)$

the gamma function. As mentioned, for $\tilde{U}_0 \leq 1$ the solution is no longer normalizable. For $\tilde{U}_0 > 1$, the steady-state second moment is

$$\langle p^2 \rangle = \begin{cases} 1/(\tilde{U}_0 - 3) & \text{for } \tilde{U}_0 > 3, \\ \infty & \text{for } \tilde{U}_0 < 3. \end{cases} \quad (12)$$

The divergence of the steady-state kinetic energy $\langle p^2 \rangle$ as \tilde{U}_0 approaches the critical value 3 from above is the direct result of the power-law tail of the momentum distribution, which in turn is due to the weak friction force at large momentum $f(p) \sim -1/p$. The key insight is that for these types of systems the difference between the steady-state distribution and the distribution at a large but finite time is non-negligible, in contradistinction to what happens for the standard $f(p) \sim -p$ friction force. While the bulk of the distribution is given correctly by the steady-state solution, the power-law tail of the time-dependent $W(p, t)$ does not extend to infinite momentum. As in the case of free diffusion in momentum space where the momentum rarely exceeds $\sim \sqrt{t}$, so too here the power-law tail is cut off at $|p| \sim \sqrt{t}$. To see this, an analysis of the dimensionless Fokker-Planck equation

$$\frac{\partial W}{\partial t} = \left(\frac{1}{\tilde{U}_0} \frac{\partial^2}{\partial p^2} + \frac{\partial}{\partial p} \frac{p}{1+p^2} \right) W \quad (13)$$

$$h(z) \sim \begin{cases} \mathcal{N} z^{-\tilde{U}_0}, & z \ll 2/\sqrt{\tilde{U}_0}, \\ \{\mathcal{N}(4/\tilde{U}_0)^{(1-\tilde{U}_0)/2} / \Gamma[(\tilde{U}_0 + 1)/2]\} z^{-1} e^{-\tilde{U}_0 z^2/4}, & z \gg 2/\sqrt{\tilde{U}_0}. \end{cases} \quad (17)$$

The Gaussian factor found for large z stems from the diffusion in momentum space as the force becomes negligible for a large momentum $p \gg \sqrt{t}$. The small- z behavior is a power law that matches the large- p behavior of the steady state of Eq. (11).

The solution $h(z)$ is non-normalizable since $h(z) \sim z^{-\tilde{U}_0}$ for small z . This type of solution is called an infinite covariant density. It is *covariant* in the sense that $z = p/\sqrt{t}$; hence, p must be scaled with the square root of time [namely, $h(z)$ remains unchanged as both \sqrt{t} and p are modified, keeping their ratio fixed], while the normalized steady state [Eq. (8)] is time invariant. Note especially that the term *infinite* refers to the non-normalizability of the solution. Thus, $h(z)$, while remaining positive, is not a probability

was presented by Levine, Mukamel, and Schütz (2005), Kessler and Barkai (2010), and Dechant, Lutz, Barkai, and Kessler (2011), who employed the scaling ansatz

$$W(p, t) \sim t^q h(p/\sqrt{t}), \quad (14)$$

which holds for a large momentum and long times. Using the diffusive scaling variable $z = p/\sqrt{t}$, the following equation is found:

$$\frac{1}{\tilde{U}_0} \frac{d^2 h}{dz^2} + \left(\frac{1}{z} + \frac{z}{2} \right) \frac{dh}{dz} - \left(q + \frac{1}{z^2} \right) h = 0. \quad (15)$$

Matching this solution to the steady-state solution that holds for $p \ll \sqrt{t}$ gives $q = -\tilde{U}_0/2$ and

$$h(z) = \frac{\mathcal{N} z^{-\tilde{U}_0}}{\Gamma[(\tilde{U}_0 + 1)/2]} \Gamma\left(\frac{1 + \tilde{U}_0}{2}, \frac{\tilde{U}_0 z^2}{4}\right), \quad (16)$$

where $\Gamma(a, x)$ is the incomplete gamma function. In the small and large z limits,

density. Its statistical meaning can be understood following the mathematical literature on infinite ergodic theory (Aaronson, 1997). In a long-time, large momentum limit with p/\sqrt{t} fixed,

$$\lim_{\substack{p, t \rightarrow \infty \\ p/\sqrt{t} \text{ fixed}}} t^{\tilde{U}_0/2} W(p, t) = h(p/\sqrt{t}). \quad (18)$$

The right-hand side of Eq. (18) is not normalized, since the perfectly normalized PDF $W(p, t)$ is multiplied by $t^{\tilde{U}_0/2}$, which diverges as $t \rightarrow \infty$. The function $h(z)$ can be used to compute the moments of the process $p(t)$, namely, those that diverge with respect to the integration over the steady state. For example, the second moment is

$$\langle p^2 \rangle = \begin{cases} 1/(\tilde{U}_0 - 3), & \tilde{U}_0 > 3, \\ \{14\mathcal{N}/2\tilde{U}_0 \Gamma[(\tilde{U}_0 + 1)/2]\} [1/(2 - \tilde{U}_0)] (t/\tilde{U}_0)^{(3-\tilde{U}_0)/2}, & 1 < \tilde{U}_0 < 3, \\ 2(1 - \tilde{U}_0)/\tilde{U}_0 t, & \tilde{U}_0 < 1. \end{cases} \quad (19)$$

For $\tilde{U}_0 > 3$ the kinetic energy is time independent, is determined by the steady-state solution, and blows up as $\tilde{U}_0 \rightarrow 3$. For the intermediate range $1 < \tilde{U}_0 < 3$, the

behavior is subdiffusive and the infinite density determines the kinetic energy. Even though for $\tilde{U}_0 < 1$ the system is actually heating linearly with time, the infinite kinetic

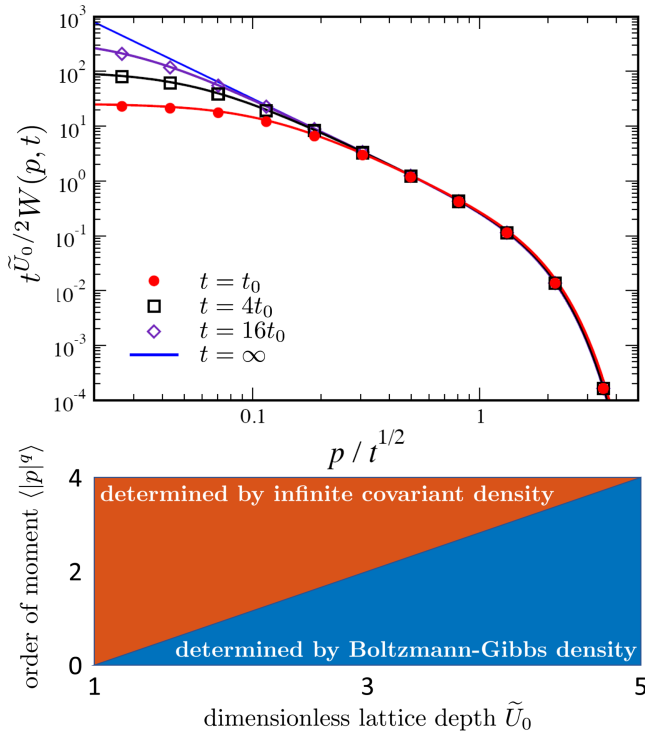


FIG. 4. Top panel: temporal dynamics of the momentum distribution. The rescaled density of momentum vs $p/t^{1/2}$ obtained from Langevin simulations [Eq. (10)] with $\tilde{U}_0 = 2$ for rescaled times $t = t_0 \equiv 76.3$, $t = 4t_0$, and $t = 16t_0$, emphasizing the large momentum of the atom where the scaling is effectively diffusive, as the friction is small. The theoretical curve is the infinite covariant density of Eq. (16), a valid description in the long-time limit. It exhibits a Gaussian-like cutoff that renders the moments finite, unlike those of the formal steady state, which diverge. Adapted from Kessler and Barkai, 2010. Bottom panel: the q th moment of the momentum as a function of \tilde{U}_0 , showing the complementarity of the two densities in calculating moments of the observables. The steady state [Eq. (11)] is termed Boltzmann-Gibbs since it describes an effective motion in a logarithmic potential (see the text). Adapted from Holz, Dechant, and Lutz, 2015.

energy of Eq. (12) is never obtained. At the critical value $\tilde{U}_0 = 1$ the system transitions to normal diffusive scaling of the mean-squared momentum. Simulations and calculations taking account of the underlying lattice structure of the laser field were performed by Holz, Dechant, and Lutz (2015). These simulations solved the relevant set of stochastic differential equations for shallow lattices, thereby showing agreement with the infinite covariant density of Eq. (16) and proving that the lattice structure does not affect the scaling properties of the system.

Infinite densities are important in many applications beyond Sisyphus cooling, in particular, in chaos theory (Akimoto, 2008; Korabel and Barkai, 2009). They have been studied extensively in the context of infinite ergodic theory (Aaronson, 1997) where the behavior of time averages is important. For the system at hand, the steady-state solution and the infinite covariant density are complementary tools, as both are long-time solutions of the problem. $W(p, t)$

converges toward the steady state as long as $\tilde{U}_0 > 1$. Similarly, plotted in the scaling form the solution approaches the non-normalized infinite density (Fig. 4). For $1 < \tilde{U}_0 < 3$, the steady-state solution predicts an infinite energy but a finite normalization, and the infinite density gives a finite energy but infinite normalization. Hence, both tools are required for a complete description of the dynamics [Fig. 4 (bottom panel)].

Consider now the case of $\tilde{U}_0 < 1$. The steady state [Eq. (11)] is not normalizable, an infinite invariant density describes the momentum distribution in the inner region $p < \sqrt{t}$, and there is a limit

$$\lim_{t \rightarrow \infty} t^{(1-\tilde{U}_0)/2} W(p, t) \sim (1 + p^2)^{-\tilde{U}_0/2}. \quad (20)$$

The expression on the right-hand side of Eq. (20) is a non-normalizable function since $\tilde{U}_0 < 1$; however, it still describes a long-time limit of the density (Dechant, Lutz, Barkai, and Kessler, 2011). The divergence emanates from the large- p behavior. Since the right-hand side of Eq. (20) is time independent, it is termed invariant and not covariant, as was the case for Eq. (18). It is not a coincidence that this is similar to the form found for the normalized steady state [Eq. (11)]. Here infinite ergodic theory comes into play, distinguishing between two types of observables: those that are integrable with respect to the non-normalized density [given by the time-independent right-hand side of Eq. (20)] and those that are not.⁷

This is similar to the kinetic energy observable considered for the case in which $\tilde{U}_0 > 1$, which, depending on the value of \tilde{U}_0 , may be either integrable or nonintegrable with respect to the infinite covariant density. The fluctuation behavior of the time averages of observables was studied by Aghion, Kessler, and Barkai (2019). The mean of the time averages can be evaluated from the non-normalized state, at least for observables that are integrable with respect to the infinite density. This is somewhat similar to the usual ergodic theory, where time averages are calculated with ensemble averages; however, now instead of using a normalized distribution in the steady state, a non-normalizable function is used. When the Darling-Kac theorem (Darling and Kac, 1957) and infinite ergodic theory is employed, it is found that certain observables, when time averaged, have a universal distribution that in turn is related to Lévy statistics (Aaronson, 1997; Aghion, Kessler, and Barkai, 2019). The details of this, however, extend beyond the scope of this Colloquium.

The regime $\tilde{U}_0 < 1$ is predicted to exhibit special features, and experiments in this region are technically challenging due to the fact that the system is actually being heated and atoms are easily lost from the trap. The issue of heating and loss of atoms can be partially mediated by use of elongated dipole “tube” traps or blue-detuned optical box potentials (Sagi et al., 2012; Afek et al., 2017, 2020; Navon, Smith, and Hadzibabic,

⁷To better understand the concept of integrability, consider a PDF $f(x)$ of a finite random variable x and an observable $O(x)$. If the integral $\int_{-\infty}^{\infty} O(x)f(x)dx$ is finite, then the observable $O(x)$ is integrable. A similar concept is used even when the system is described by a non-normalized state.

2021); however, to date there has been no clear-cut experimental proof of Eq. (20).

The meaning of temperature.—When a gas is coupled to a heat bath, its equilibrium temperature is proportional to the variance of its momentum distribution, which is Gaussian. How, then, does one define a temperature for the Sisyphus-cooled system? One approach is that there is no temperature at all since the system is in a nonequilibrium state. On a more practical level, though, a temperature-like quantifier typically used in experiments can be defined that is the full width at half maximum (FWHM) of the momentum distribution. A third option is to use the mean of the kinetic energy, which is equivalent in equilibrium to the normal temperature. For shallow lattices, this observable should be obtained from the infinite invariant density and not from the steady state. Furthermore, in the shallow-lattice regime the distribution can have a narrow FWHM but also a variance that increases with time. This means that one measure of the temperature (FWHM) can indicate that the system is cold, while another can indicate that it is hot.

Diffusion in a logarithmic potential.—The problem of momentum dynamics of Sisyphus-cooled ultracold atoms is related to the overdamped Langevin dynamics in a logarithmic potential (Poland and Scheraga, 1966; Bray, 2000; Bar, Kafri, and Mukamel, 2007; Fogedby and Metzler, 2007a, 2007b; Bar, Kafri, and Mukamel, 2009; Dechant, Lutz, Kessler, and Barkai, 2011; Hirschberg, Mukamel, and Schütz, 2011, 2012; Ray and Reuveni, 2020). Intuitively, this connection stems from the fact that the friction force $f(p) \sim -1/p$ at large p , and hence asymptotically the effective potential in momentum space is $V(p) = -\int dp f(p) \sim \log(p)$. More explicitly, consider a Brownian particle in a potential $V(x) = V_0 \log(1 + x^2)$ in contact with a standard thermal heat bath with temperature T . According to the Boltzmann-Gibbs framework, the density in thermal equilibrium is $P_{\text{eq}} = \mathcal{N}(1 + x^2)^{-V_0/k_B T}$, bearing the same structure of the steady-state equation (8) with appropriate adjustments. The stochastic dynamics in a log potential is important for several problems, like DNA looping (Hanke and Metzler, 2003; Bar, Kafri, and Mukamel, 2007) and Manning condensation (Manning, 1969).

B. Position space

An immediate consequence of the anomalous dynamics in momentum space is nontrivial dynamics in position space. Marksteiner, Ellinger, and Zoller (1996) theoretically studied the spatial diffusion of atoms and revealed that below a critical depth of the optical lattice there is a transition to Lévy-like motion. To show this, certain modifications of the basic Lévy walk are needed. Consider a long-time momentum-space trajectory $p(t)$, crossing zero many times. Let τ be the random interval of time between two successive such crossings, and let χ be the random displacement for a given such interval (schematically presented in Fig. 5). A process is generated with a set of random jump durations $\{\tau_i\}$ between zero crossings and corresponding displacements $\{\chi_i\}$ given by $\chi_1 = \int_0^{\tau_1} dt p(t)$, $\chi_2 = \int_{\tau_1}^{\tau_1+\tau_2} dt p(t)$, etc. For a particle starting at the origin at $t=0$ with $p=0$, the sum of all the displacements χ_i is the random position of the particle at

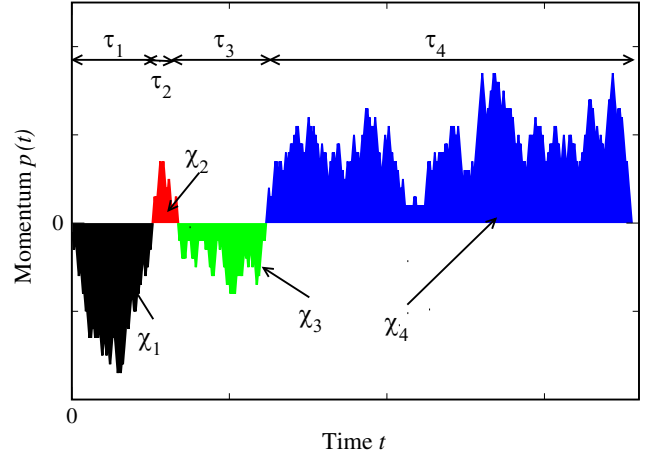


FIG. 5. The nature of the spatial diffusion is revealed by numerical simulation of momentum zero-crossing dynamics. The crossing of zero momentum defines the durations τ_i and jump distances χ_i , enabling identification of the connection between the continuous momentum trajectory of the atom and the Lévy walk picture. The jump distances are the areas under the stochastic momentum curve that starts and ends at zero momentum and never crosses in between. The time periods between the zero crossings are indicated by the black arrows at the top. Adapted from Kessler and Barkai, 2012.

time $t = \sum_i \tau_i$, denoted $x(t)$, and the corresponding PDF is $P(x, t)$. Since the Langevin process [Eq. (10)] is driven by white noise, defining zero crossings requires a more precise treatment (Majumdar and Comtet, 2004, 2005; Kessler and Barkai, 2012; Barkai, Aghion, and Kessler, 2014). We define the random time τ as the time it takes the particle starting with momentum $p = \epsilon$ to reach $p = 0$ for the first time.

The Langevin process of Eq. (10) is Markovian, so once the particle crosses zero momentum a given interval τ is independent of the previous one. This is simply a renewal process: τ_i is drawn repeatedly from $\psi(\tau)$, the crossing time PDF computed using the Langevin equation (10), until the sum of the times exceeds the measurement time. The distribution of crossing times can be calculated using the tools of first-passage theory (Redner, 2001; Micciché, 2010; Martin, Behn, and Germano, 2011). The marginal PDFs of step durations and jump distances exhibit power-law behaviors (Marksteiner, Ellinger, and Zoller, 1996; Barkai, Aghion, and Kessler, 2014),

$$\psi(\tau) \sim \tau^{-(3/2) - \tilde{U}_0/2}, \quad q(\chi) \sim |\chi|^{-(4/3) - \tilde{U}_0/3}. \quad (21)$$

Equation (21) is the result of the weak friction found at large momentum. In the limit $\tilde{U}_0 = 0$, $\psi(\tau) \sim \tau^{-3/2}$, which describes the distribution of first-passage times of a Brownian particle in 1D searching for a target at the origin (Redner, 2001). This extremely shallow-lattice limit describes a pure diffusive process in momentum space with no friction. Long intervals are associated with large momenta, so the cooling friction does not destroy the existence of power-law decay at large τ , though it does change the actual exponent. The mean of τ diverges when $\tilde{U}_0 \leq 1$, and the mean first-passage time for the momentum, namely, the time it takes the momentum to

cross the origin, becomes infinite when the steady state of the momentum distribution equation (11) is no longer normalized.

These scaling results suggest a transition between a standard, Gaussian, random-walk regime and a Lévy regime as \tilde{U}_0 goes below 5. For $\tilde{U}_0 > 5$, the variance of χ is finite [since $q(\chi) \sim |\chi|^{-3}$ when $\tilde{U}_0 = 5$], so, based on the central limit theorem argument presented in Sec. II.A, a Gaussian position distribution of $P(x, t)$ is expected to be obtained in the long-time limit. For $\tilde{U}_0 < 5$, on the other hand, the variance of χ diverges, suggesting a Lévy flight scenario (at least as long as $\tilde{U}_0 > 1$ and the mean flight duration τ is finite). $P(x, t)$ attains the following self-similar scaling form:

$$P(x, t) \sim \frac{1}{(K_\nu t)^{1/\nu}} L_{\nu,0} \left[\frac{x}{(K_\nu t)^{1/\nu}} \right]. \quad (22)$$

In Eq. (22) $L_{\nu,0}(x)$ is the symmetric Lévy stable PDF of Eq. (4). The transport coefficient K_ν describes the width of the packet and is given in terms of the microscopic parameters of the model (Kessler and Barkai, 2012). The Lévy exponent $\nu = (\tilde{U}_0 + 1)/3$ is such that the solution approaches a Gaussian when $\tilde{U}_0 \rightarrow 5$. K_ν vanishes as $\tilde{U}_0 \rightarrow 1$ due to the divergence of the average τ .

As discussed in Sec. II.A, power-law tails lead to infinite moments, and hence the Lévy law in Eq. (22) as a stand-alone solution is not valid for a large x and a finite time. The resolution of this paradox lies in the fact that the random variables τ and χ are in fact correlated since longer flight durations lead to larger displacements. In fact, the largest jump in the process $p(t)$ cannot be much larger than a length scale that increases as $t^{3/2}$, beyond which the tails of the Lévy PDF are naturally cut off. This is made evident by completely neglecting the restoring friction force. The momentum then undergoes pure diffusion, scaling like $t^{1/2}$, and the jump size scales accordingly as $t^{3/2}$. This is a kind of Lévy walk rather than a Lévy flight. It is unlike the original Lévy walk, where the largest jump scales linearly with measurement time, since here the velocity is constant between turning points, whereas here the motion is stochastic between any two zero crossings. This spatial regime, where the Lévy density [Eq. (22)] holds, is therefore valid only up to a length scale that grows like $t^{3/2}$. This Lévy regime also shrinks as \tilde{U}_0 increases and vanishes as $\tilde{U}_0 \rightarrow 5$, beyond which only the Gaussian regime survives. To handle these correlations, a tool called the Montroll-Weiss equation (Montroll and Weiss, 1965) has to be employed (Metzler and Klafter, 2000; Zaboradaev, Denisov, and Klafter, 2015). It relates the joint PDF of jump distances and waiting times to the density of particles $P(x, t)$ using the convolution theorem of the Laplace and Fourier transforms. Going through the analysis of the Montroll-Weiss equation, it is indeed found that Eq. (22) is valid in the central regime (Fig. 6).

An analysis of the far tail of $P(x, t)$ was carried out by Aghion, Kessler, and Barkai (2017), who found a spatial infinite (i.e., non-normalized) density. The analysis showed a relation between the laser-cooling process and the problem of the distribution of random areas under Langevin excursions (Majumdar and Comtet, 2005; Barkai, Aghion, and Kessler, 2014; Agranov et al., 2020). The latter is a constrained

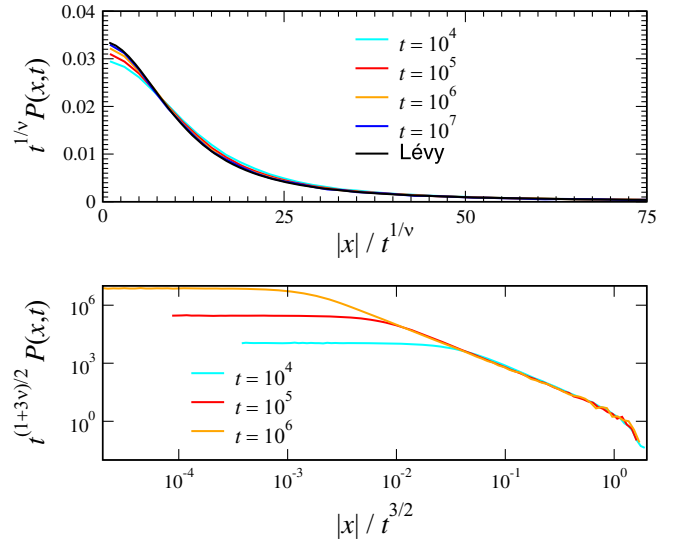


FIG. 6. Langevin simulations of the spatial dynamics. Top panel: results of numerical simulations of Eq. (10). Packets of particles starting from a common origin converge in the long-time limit to a self-similar Lévy density that is presented as a solid line [Eq. (22); $\nu = 7/6$]. Bottom panel: the simulated distribution also exhibits a second scaling, i.e., data collapse for several measurement times. The convergence is faster for large $x/t^{3/2}$, while for small values deviations from the scaling are found. At large distances the power-law decay of the Lévy density is cut off due to finite time effects. Adapted from Kessler and Barkai, 2012.

Langevin process starting and ending at $p = 0$ that never crosses the origin within a given time interval (Fig. 5). The derived cutoff of $P(x, t)$ due to the aforementioned correlations ending the power-law Lévy regime can be seen at the far right edge of the bottom panel of Fig. 6 and is in accord with direct simulations of the Langevin equation (10).

When $\tilde{U}_0 < 1$, the correlations between the walk duration and distance can never be neglected and then $P(x, t) \sim (1/t^{3/2})g(x/t^{3/2})$, where g is a scaling function. In this limit of shallow lattices, the momentum performs a random walk due to the random emission events, the friction is negligible, and the momentum scales like \sqrt{t} , as in Eq. (19). Hence, as shown analytically by Barkai, Aghion, and Kessler (2014), a cubic scaling of the MSD is obtained. This type of Richardson-like behavior, measured originally by Richardson (1926) following the distance between two weather balloons in a turbulent atmosphere, was found by Wickenbrock et al. (2012) using Monte Carlo simulations, and the phase $\tilde{U}_0 < 1$ is called the Richardson phase. Richardson's law has thus far evaded measurement in atomic systems but has been experimentally observed in other contexts (Duplat et al., 2013).

The MSD therefore has three distinct phases, normal diffusion, superdiffusion, and Richardson diffusion:

$$\langle x^2 \rangle \sim \begin{cases} t, & 5 < \tilde{U}_0, \\ t^{(7-\tilde{U}_0)/2}, & 1 < \tilde{U}_0 < 5, \\ t^3, & \tilde{U}_0 < 1. \end{cases} \quad (23)$$

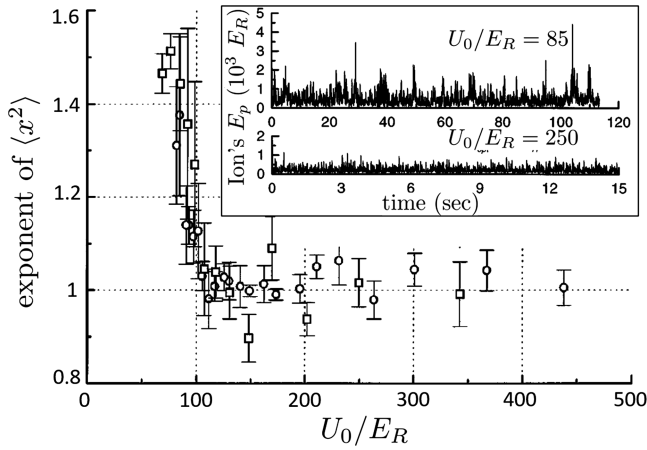


FIG. 7. Exponent of the MSD $\langle x^2 \rangle$ experimentally measured using the dynamics of a weakly harmonically trapped single $^{24}\text{Mg}^+$ ion in a Sisyphus lattice. For deep lattices, the dynamics is diffusive and $\langle x^2 \rangle \sim t$. As the lattice becomes shallower, a steep rise in the exponent is observed as the dynamics becomes superdiffusive [Eq. (23)]. Inset: time traces of the potential energy of the ion displayed as it moves in the trap. Large rare events are visible in the shallow lattice (top) corresponding to the heavy tails of the distributions, which are compared to the more Gaussian behavior of the deep lattice data (bottom). Adapted from Katori, Schlipf, and Walther, 1997.

This behavior differs from the original Lévy walk picture of Eq. (5), which exhibits at most ballistic spreading. An intuitive argument for the behavior of the MSD in the regime $1 < \tilde{U}_0 < 5$ can be obtained by considering that the Lévy distribution of Eq. (22) describes the central part of the packet and that a cutoff exists at distances of the order of $t^{3/2}$ (Fig. 6). From the power-law tail of the distribution, $P(x, t) \simeq tx^{-1-\nu}$ for $x < t^{3/2}$ can be obtained. We then get $\langle x^2 \rangle \simeq \int t^{3/2} dx x^2 P(x, t)$, and using $\nu = (\tilde{U}_0 + 1)/3$ the result of Eq. (23) is found. In short, the cutoff of the spatial Lévy distribution gives the correct time dependence of the MSD, but to calculate the MSD precisely, including prefactors, one needs to resort to the scaling Green-Kubo theory investigated in Sec. IV.A.

The transition from normal to anomalous diffusion was observed experimentally by Katori, Schlipf, and Walther (1997), where the axial motion of a single $^{24}\text{Mg}^+$ ion trapped in a quadrupole ring trap undergoing one-dimensional Sisyphus cooling brought about by a pair of slightly red-detuned counterpropagating laser beams was used to measure the MSD. The position of the ion was continuously measured by detecting its fluorescence photons through a high numerical aperture microscope objective to within a spatial resolution of $3 \mu\text{m}$ and a temporal resolution of 10 ms. The scaling exponent of the MSD was observed to rise above unity below some threshold value of \tilde{U}_0 , continuing to rise with decreasing \tilde{U}_0 . The rise was roughly linear with \tilde{U}_0 , and the slope was consistent with the theoretical prediction of unity. Figure 7 depicts the exponent of the MSD of the trapped ion, as well as its time traces showing a clear transition from normal statistics for deep lattices to rare-event dominated statistics for shallow ones.

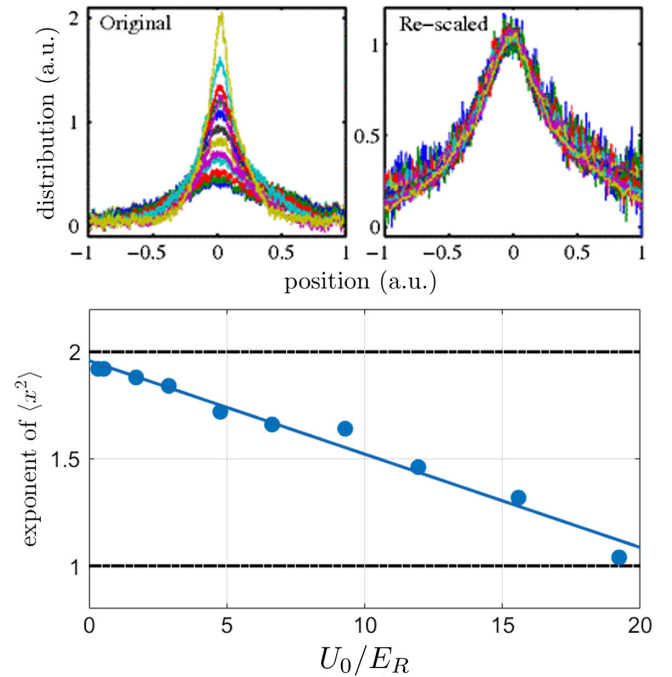


FIG. 8. Self-similarity, Lévy distributions, and superdiffusion. The temporal scaling of the spatial distribution is experimentally measured in one dimension. Top panel: data collapse of the spatial distributions as a function of time, indicated in different colors, for the rescaling transformation $x \rightarrow x/t^{1/\nu}$ [Eq. (22) and Fig. 6], with $\nu = 1.25$ in a $U_0/E_R = 4.8$ lattice. Bottom panel: extracted exponent of the MSD $\langle x^2 \rangle$. C of Eq. (9) is used as a fitting parameter for Eq. (23), giving a value of 11 ± 1 for this measurement. The experiment also observed the power-law tails of the spatial distribution predicted by Eq. (22). Adapted from Sagi et al., 2012.

The spatial dynamics was further explored by Sagi et al. (2012), where the 1D diffusion of cold ^{87}Rb atoms undergoing Sisyphus cooling was studied. Starting with a narrow, thermally equilibrated atomic cloud,⁸ the particles were released and their density profile absorption imaged. To enable long-time measurements of the 1D dynamics and minimize the escape of atoms into other orthogonal dimensions, a far-detuned tube-dipole trap was used with a geometry that generated strong confinement on the radial axes but a negligible effect on the experimental axis as defined by the Sisyphus lattice beams.

In qualitative agreement with theory, a transition from normal to anomalous dynamics was observed and Lévy distributions were found to fit well to the experimental data, confirming the transition between the normal Gaussian diffusion regime for deep enough lattices and the Lévy regime below some critical \tilde{U}_0 . Both the power-law scaling of the MSD and the Lévy distribution of the displacement, with the Lévy index changing with lattice depth, were observed, in agreement with theory. The scaling collapse and the resultant Lévy distributions are shown in the top panel of Fig. 8.

⁸This is achieved by allowing a long evaporation time where collisions thermalize the atomic cloud. The momentum distributions after the evaporation stage are verified to be Gaussian with a variance corresponding to a temperature of $12 \mu\text{K}$.

The bottom panel shows the measured exponent of the time-dependent MSD as a function of U_0/E_R . The superdiffusive nature of the spatial spreading is also in agreement with the theoretical expectations. In addition, the linear dependence of the exponent with U_0/E_R is in agreement with Eq. (23).

This agreement between theory and experiment, while encouraging, remains incomplete. In particular, exponents above 2 and the saturation at a value of 3 associated with the Richardson phase have yet to be observed. This is not totally unexpected, since if the particles are moving superballistically they will quickly leave the trap and may go undetected (Sagi *et al.*, 2012). A possible way to alleviate this may arise in the form of optically engineered potentials that create strong confinement as well as reflecting boundary conditions for the atomic packet (Gaunt *et al.*, 2013; Livneh, Afek, and Davidson, 2018).

C. Position-momentum correlations

As both the momentum [Eq. (19)] and position [Eq. (23)] dynamics are governed by power laws, the cross-correlation C_{xp} between position and momentum may be expected to behave in a similar way. Defined according to

$$C_{xp}(t) = \frac{\langle x(t)p(t) \rangle}{\sqrt{\langle x^2(t) \rangle \langle p^2(t) \rangle}}, \quad (24)$$

this function asymptotically decays as $1/\sqrt{t}$ for normal diffusion (Gillespie and Seitaridou, 2012) and approaches unity for ballistic motion. This observable is in general challenging to access experimentally, as it requires knowledge of the position of a group of atoms contained in a certain narrow momentum bin.

Afek *et al.* (2017) derived a scaling relation describing the asymptotic dynamics of $C_{xp}(t \rightarrow \infty)$ for the general case where both the position and the momentum have power-law long-time behavior: $\langle x^2(t) \rangle \sim t^{2\alpha_x}$ and $\langle p^2(t) \rangle \sim t^{2\alpha_p}$. Here the exponents α_i describe anomalous processes in general. Substituting them into Eq. (24), along with the fact that $\langle xp \rangle \sim d\langle x^2 \rangle / dt \sim t^{2\alpha_x - 1}$, gives $C_{xp} \sim t^{\alpha_x - \alpha_p - 1}$. In terms of \tilde{U}_0 , it should then scale as

$$C_{xp}(t) \sim \begin{cases} \text{const}, & \tilde{U}_0 < 3, \\ t^{(3-\tilde{U}_0)/4}, & 3 < \tilde{U}_0 < 5, \\ t^{-1/2}, & \tilde{U}_0 > 5. \end{cases} \quad (25)$$

As \tilde{U}_0 is varied, the behavior ranges from normal, a $t^{-1/2}$ decay, to a constant. This has been numerically verified in an analysis of the simulations performed by Afek *et al.* (2017) and is shown in the bottom panel of Fig. 9.

The correlation function, however, is not merely a tool to explore the long-time dynamics. Rather, it yields information about the short-time behavior as well. An additional feature discussed by Afek *et al.* (2017) relates to the short-time dynamics of a system of particles released from a harmonic trap and allowed to propagate in the Sisyphus lattice. At times that are short compared to the oscillation period in the trap before release ($t < 1/\omega$), correlations build up linearly regardless of the depth of the lattice, as the diffusive dynamics

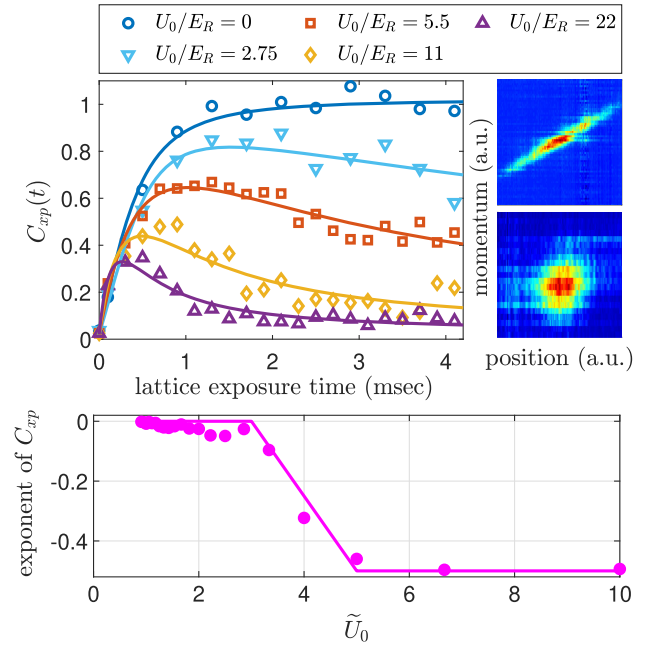


FIG. 9. Anomalous dynamics in momentum and position leads to interesting position-momentum correlations. Top panels: experimental results for the position-momentum correlations as a function of lattice exposure time and lattice depth U_0/E_R . At short times the correlations build up and are later quenched at varying rates, depending on the anomalous dynamics. The images on the right are the tomographically measured phase-space probability densities for ballistic expansion (upper panel) and $U_0/E_R = 5.5$ (lower panel), at a lattice exposure time of 4.1 ms, showing the effect of the lattice on the development of the correlations. Bottom panel: Langevin simulation (circles) validating the prediction of Eq. (25) depicted as a solid line. Adapted from Afek *et al.*, 2017.

do not yet affect the atoms (ω sets, in accordance with the equipartition theorem, the ratio between the initial standard deviation of the momentum distribution and that of the position distribution). At longer times, diffusion kicks in and the behavior of Eq. (25) is expected to take over.

A setup similar to that described by Sagi *et al.* (2012) was used to generate the anomalous dynamics, and a method based on velocity-selective two-photon Raman transitions (Moler *et al.*, 1992) was developed to tomographically image the phase-space density distribution function. In this method, atoms contained within a narrow velocity class are selectively transferred from the $|F = 1\rangle$ lower hyperfine state to the upper $|F = 2\rangle$ state using a Raman π pulse of a given detuning. The center of the selected velocity class is scanned by varying the two-photon detuning of the pulse, and the Rabi frequency sets its width (Kasevich *et al.*, 1991). The position of the selected atoms is then directly imaged using state-selective absorption imaging. This way, a direct measurement of the position-momentum correlation function is enabled for different initial conditions given by the Sisyphus lattice exposure. The two right panels at the top of Fig. 9 are experimental reconstructions of the phase-space density distributions. The upper panels reveal a high correlation corresponding to ballistic expansion, while the lower panel shows the destruction of the correlation by the diffusive dynamics.

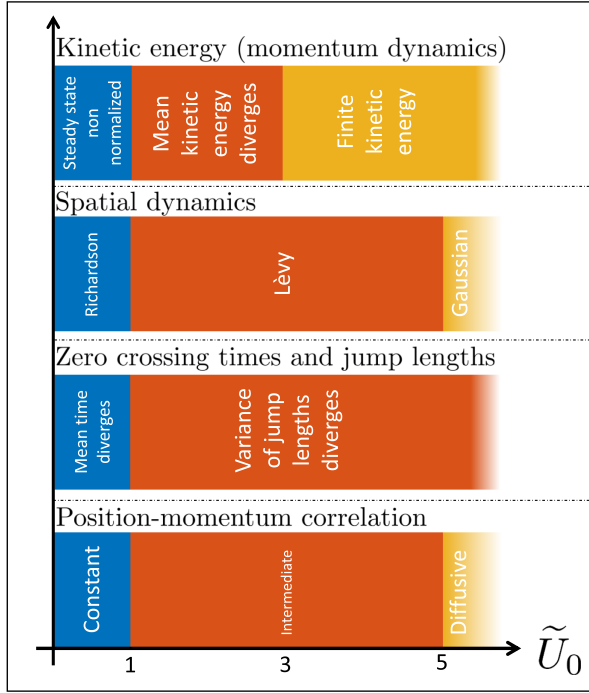


FIG. 10. Recap of the dynamical phases for various observables. Varying the experimentally accessible control parameter \tilde{U}_0 defined in Eq. (9) and Fig. 2 reveals transitions in the statistical properties of the system discussed in Sec. III. Momentum, position, and position-momentum correlations all display sharp transitions between different regimes. Nonphysical divergences are resolved when moments are calculated using the formalism of the infinite covariant density.

Figure 9 (top panels) shows the dynamics of these correlations as an atomic cloud evolves in lattices of different \tilde{U}_0 . The initial buildup of the correlation is evident for all lattice depths considered, as well as the following decay. The $\tilde{U}_0 = 0$ dataset is expected (and shown) to be ballistic.

The various aspects discussed in this section can be summarized in the form of a “phase diagram.” Figure 10 presents the dependence of the momentum [Eq. (19)] and spatial dynamics [Eq. (23)] on the lattice depth parameter \tilde{U}_0 defined in Eq. (9), as well as changes in the statistical properties of momentum zero-crossing times and jump distances [Eq. (21)] and even the position-momentum correlation [Eq. (25)]. All of these display sharp transitions between various regimes as \tilde{U}_0 is scanned.

IV. IMPLICATIONS FOR FUNDAMENTAL CONCEPTS IN STATISTICAL PHYSICS

A. Scaling Green-Kubo relation

As mentioned in Sec. I, the Green-Kubo relation, which was first discussed by Taylor (1922) in the context of diffusion in a turbulent medium, relates the diffusion constant of a particle $D = \langle x^2(t) \rangle / 2t$ to an integral over the stationary time correlation function of the momentum $C_p(t, t + \tau) = \langle p(t)p(t + \tau) \rangle$ (Green, 1954; Kubo, 1957). For a particle with mass M ,

$$D = \frac{1}{M^2} \int_0^\infty d\tau C_p(t, t + \tau). \quad (26)$$

In the case of a Brownian particle with a Stokes friction coefficient γ_s , the momentum correlation function $C_p(t, t + \tau) = k_B T M e^{-\gamma_s \tau}$ is exponential. The Green-Kubo formula gives the Einstein relation $D = k_B T / M \gamma_s$ linking the diffusivity and the friction coefficient via the temperature T . In the Sisyphus-cooled atomic system at hand, for $\tilde{U}_0 > 3$ this standard Green-Kubo relation applies. For $\tilde{U}_0 < 3$, however, it breaks down for one of two reasons: either the correlation function is not stationary or, alternatively, while the correlation function is stationary, its time integral diverges. Depending on the value of \tilde{U}_0 , either scenario can occur, and in both cases Eq. (26) needs to be generalized. This is done following Dechant *et al.* (2014).

Consider the general momentum correlation function

$$C_p(t_2, t_1) = \int_{-\infty}^{\infty} dp_2 \int_{-\infty}^{\infty} dp_1 p_2 p_1 P(p_2, t_2 | p_1, t_1) P(p_1, t_1 | 0, 0), \quad (27)$$

where $P(p_2, t_2 | p_1, t_1)$ is the probability of the particle having momentum p_2 at time t_2 given that it had momentum p_1 at time t_1 . The notation $P(p_2, t_2 | p_1, t_1)$ is used here, as opposed to the $W(p, t)$ used earlier, to explicitly indicate the dependence on the initial momentum and time. $\langle x^2(t) \rangle$ can then be calculated from $C_p(t_2, t_1)$. In the case where the process is stationary at long times, such that the stationary momentum distribution (denoted by the subscript s) exists and is given by $\lim_{t_1 \rightarrow \infty} P(p_1, t_1 | 0, 0) = W_s(p_1)$, then $C_p(t_2, t_1) = C_{p,s}(|t_2 - t_1|)$ depends only on the time lag $\tau = t_2 - t_1$,

$$C_{p,s}(\tau) = \int_{-\infty}^{\infty} dp_2 \int_{-\infty}^{\infty} dp_1 p_2 p_1 P(p_2, \tau | p_1, 0) W_s(p_1). \quad (28)$$

Since $x(t)$ is the time integral of $p(t)/M$,

$$\begin{aligned} \langle x^2(t) \rangle &= \frac{1}{M^2} \int_0^t dt_2 \int_0^{t_2} dt_1 C_{p,s}(|t_2 - t_1|) \\ &= \frac{2t}{M^2} \int_0^\infty d\tau C_{p,s}(\tau), \end{aligned} \quad (29)$$

from which follows the standard Green-Kubo formula [Eq. (26)].

What then is the form of the momentum correlator $C_p(t_2, t_1)$ in the Sisyphus system? Turning to the definition of Eq. (27), we have already seen how to calculate from the Fokker-Planck equation (7) the factor $W(p_1, t_1)$. For large p_1 , this decays as a power law with a Gaussian falloff at $p_1 \sim O(\sqrt{t_1})$ [Eqs. (14), (16), and (17)]. The calculation of the other factor $P(p_2, p_1; t_2 - t_1)$ is similar and behaves similarly for large p_2 as long as p_1 is not too large, which is the relevant regime since the $P(p_1, t_1 | 0, 0)$ factor in Eq. (27) cuts it off. A detailed calculation (Dechant, Lutz, Kessler, and Barkai, 2011; Dechant *et al.*, 2012) revealed that the correlator has the following form:

$$C_p(t_2, t_1) \approx \begin{cases} C_{\alpha>1} t_1^{2-\alpha} g_{\alpha>1}[(t_2 - t_1)/t_1], & \alpha > 1, \\ C_{\alpha<1} t_1 g_{\alpha<1}[(t_2 - t_1)/t_1], & \alpha < 1, \end{cases} \quad (30)$$

where $\alpha \equiv (\tilde{U}_0 + 1)/2$ and

$$\begin{aligned} C_{\alpha>1} &= \frac{\mathcal{N}(4D_0/p_c)^{2-\alpha} \sqrt{\pi}}{\Gamma(\alpha+1)\Gamma(\alpha)/p_c}, \\ C_{\alpha<1} &= \frac{4D_0 \sqrt{\pi}}{\Gamma(\alpha+1)\Gamma(1-\alpha)}, \\ g_{\alpha>1}(s) &= s^{2-\alpha} \int_0^\infty dy y^2 e^{-y^2} {}_1F_1\left(\frac{3}{2}; \alpha+1; y^2\right) \Gamma(\alpha, y^2 s), \\ g_{\alpha<1}(s) &= s \int_0^\infty dy y^2 e^{-y^2} {}_1F_1\left(\frac{3}{2}; \alpha+1; y^2\right) e^{-y^2 s}. \end{aligned} \quad (31)$$

${}_1F_1$ is the confluent hypergeometric function, and \mathcal{N} is the normalization factor given after Eq. (11). The correlation function is in general nonstationary. The dependence of the correlator on the relative time $s = (t_2 - t_1)/t_1$ is called aging. Normally the aging correlator has the form $\langle C_p(t_2, t_1) \rangle \sim \langle p^2 \rangle_{\text{eq}} g(s)$ (Bouchaud, 1992; Margolin and Barkai, 2004; Burov, Metzler, and Barkai, 2010); however, here it takes the form

$$C_p(t_2, t_1) \sim t_1^\phi g(s) \sim \langle p^2(t_1) \rangle g(s), \quad (32)$$

where $\phi = \min(2 - \alpha, 1)$ and $g(s)$ is either $g_{\alpha>1}$ or $g_{\alpha<1}$, depending on whether α is greater or smaller than unity. To mark this added dependence on t_1 due to the growth of $\langle p^2(t_1) \rangle$ with time, this phenomenon is termed superaging.

We now consider the limit $t_2 - t_1 \ll t_1$,

$$C_p(t_2, t_1) \approx \begin{cases} [\pi\Gamma(\alpha-2)/4\mathcal{N}\Gamma^2(\alpha-1/2)][4D_0(t_2-t_1)]^{2-\alpha}, & \alpha > 2, \\ [1/\mathcal{N}\Gamma(\alpha)\Gamma(2-\alpha)](4D_0 t_1)^{2-\alpha}, & 1 < \alpha < 2, \\ (1-\alpha)4D_0 t_1, & \alpha < 1. \end{cases} \quad (33)$$

For $\alpha > 2$, $\phi = 2 - \alpha$ and the t_1^ϕ factor cancels against the t_1 factor in $g(s)$, leaving the correlation function stationary in this limit, a fact that is important for the discussion of ergodicity breaking in Sec. IV.B. For $\alpha < 2$, on the other hand, even the limiting correlation function is nonstationary and dominated by the growth in time of $\langle p^2(t_1) \rangle$, leading to superaging.

The superaging of the correlation function [Eq. (32)] has some interesting consequences for the MSD (Dechant *et al.*, 2014). For $t \gg 1$,

$$\begin{aligned} \langle x^2(t) \rangle &\simeq \frac{2C_f}{M^2} \int_0^t dt_2 \int_0^{t_2} dt_1 t_1^\phi g\left(\frac{t_2 - t_1}{t_1}\right) \\ &\simeq \frac{2C_f}{M^2} \int_0^t dt_2 t_2^{\phi+1} \int_0^\infty ds (s+1)^{-\phi-2} g(s) \\ &\simeq 2D_\phi t^{\phi+2}, \end{aligned} \quad (34)$$

with

$$D_\phi \equiv \frac{C_f}{M^2(\phi+2)} \int_0^\infty ds (s+1)^{-\phi-2} g(s). \quad (35)$$

In Eq. (35) C_f is either $C_{\alpha>1}$ or $C_{\alpha<1}$, as appropriate. This reproduces the scaling behavior of Eq. (23) on general grounds from the Lévy scaling and the cutoff, adding to it the calculation of D_ϕ .

Equation (34) is the scaling form of the Green-Kubo relation. It is applicable for $\phi > -1$, which corresponds to superdiffusion. The usual diffusion coefficient in Eq. (26) is

then ill defined and replaced by the anomalous diffusion coefficient D_ϕ . As with the original Green-Kubo formula, D_ϕ is given in terms of an integral over a function of a single variable. Determining the diffusive behavior of a system from its correlation function thus amounts to determining the exponent ϕ and the scaling function $g(s)$. While Eq. (34) was derived in terms of the momentum and position, it holds for any two quantities where one is up to a constant factor the time integral of the other. One example of such an analogy (between frequency and phase) is given in Sec. V.A.

The different scaling regimes for the MSD for the Sisyphus problem are thus seen to be related to the properties of the correlator. For $\alpha > 3$ ($\tilde{U}_0 > 5$), the correlator is stationary, the integral in the standard Green-Kubo formula converges, and the diffusion is normal. The spatial diffusion constant diverges as $\alpha \rightarrow 3$ from above due to the factor $s^{2-\alpha}$ in g , signaling the breakdown of normal diffusion. For $1 < \alpha < 3$ ($1 < \tilde{U}_0 < 5$), the standard Green-Kubo formula breaks down and the exponent $\phi = 2 - \alpha$. The MSD then scales as $t^{4-\alpha}$ and the dynamics are superdiffusive, with an anomalous diffusion constant (plugging in the value of \mathcal{N}) given by

$$D_\phi = \frac{(4D_0)^{2-\alpha} p_c^{2\alpha-2} \Gamma(\alpha-1/2)(\alpha-1)}{\Gamma^3(\alpha)\alpha(4-\alpha)M^2} \int_0^\infty ds (s+1)^{\alpha-4} g_{\alpha>1}(s). \quad (36)$$

This vanishes at $\alpha = 1$ ($\tilde{U}_0 = 1$) and, due to the factor $s^{2-\alpha}$ in $g_{\alpha>1}(s)$, diverges as $\alpha \rightarrow 3$.

For $\alpha < 1$ ($\tilde{U}_0 < 1$) the anomalous diffusion exponent saturates at a value of 3, corresponding to Richardson diffusion. The anomalous diffusion constant in this regime is

$$D_\phi = \frac{4D_0\sqrt{\pi}}{3\Gamma(\alpha)\Gamma(1-\alpha)M^2} \int_0^\infty ds (s+1)^{-3} g_{\alpha < 1}(s). \quad (37)$$

The momentum correlation function can be directly measured using existing experimental techniques similar to those described in Sec. III.C. For example, an extremely narrow atomic momentum distribution centered around a specifically targeted momentum p_0 can be prepared using two-photon momentum-selective Raman transition with two counterpropagating, far-detuned laser beams (Kasevich *et al.*, 1991) and then exposed to Sisyphus cooling for a variable amount of time t_1 . The resulting momentum distribution $P(p)$ can then be measured again after an additional time t_2 with high resolution using the same Raman momentum selection method, directly yielding the correlation function $C_p(t_2, t_1)$, and through it the Green-Kubo relation.

B. Breakdown of ergodicity

Systems in equilibrium visit all of phase space, with the average relative frequency of visiting any certain point given by the Boltzmann-Gibbs distribution. Thus, over long enough observation times, the time averages of observables correspond to the equilibrium ensemble averages. In systems with anomalous diffusion, however, this is no longer necessarily the case (Metzler *et al.*, 2014). The time average, even in the infinite time limit, varies from realization to realization. This was studied in the context of subrecoil laser cooling (Saubaméa, Leduc, and Cohen-Tannoudji, 1999), fluorescence intermittency in quantum dots (Brokmann *et al.*, 2003), and single-atom motion in nondissipative optical lattices (Kindermann *et al.*, 2017). Ergodicity breaking in Sisyphus cooling was first theoretically investigated by Lutz (2004). An alternative analysis taking into account the essential time dependence of the momentum distribution at large momenta was given by Dechant, Lutz, Kessler, and Barkai (2011) and Dechant *et al.* (2012).

To probe the possibility of ergodicity breaking for the momentum, consider the ensemble variance of the difference between the time average \bar{p} and the ensemble average $\langle p \rangle$ for a particle that starts with momentum $p = 0$ at $t = 0$. Ergodicity is broken when $\bar{p} - \langle p \rangle$, which reduces to

$$\langle \bar{p}^2 \rangle = \lim_{t \rightarrow \infty} \frac{1}{t^2} \langle x^2 \rangle \quad (38)$$

for symmetric distributions, deviates from zero. Given Eq. (23) describing the spatial MSD, we find that (Dechant *et al.*, 2012)

$$\langle \bar{p}^2 \rangle \sim \begin{cases} t^{-1}, & \alpha > 3, \\ t^{2-\alpha}, & 1 < \alpha < 3, \\ t, & \alpha < 1. \end{cases} \quad (39)$$

The $1/t$ behavior seen for $\alpha > 3$ ($\tilde{U}_0 > 5$) is the normal behavior. For $2 < \alpha < 3$ ergodicity is achieved, albeit anomalously slower. For $\alpha < 2$, $\langle \bar{p}^2 \rangle$ does not vanish as $t \rightarrow \infty$ and ergodicity is broken.

C. Violation of the equipartition theorem

Up to this point we have focused on free, untrapped systems [with the exception of the trapped ion system of Fig. 7 (Katori, Schlipf, and Walther, 1997)]. We now address the effect of an external binding potential whose scale is much larger than the wavelength of the Sisyphus lattice and hence is not averaged out in the semiclassical treatment. Generally a violation of equipartition in this inherently nonequilibrium system might be expected. The question that then arises is as follows: Can the effect be quantified? In this case, instead of simply searching for an expected violation of equipartition, the issue becomes one of determining the relation between moments of position and momentum for the nonlinear friction under study. These have been studied theoretically, both in the simple context of a harmonic well (Dechant, Kessler, and Barkai, 2015; Dechant *et al.*, 2016) and recently in a more general context (Falasco, Barkai, and Baiesi, 2022). These works focused on the steady-state phase-space distribution of the particles and, in particular, the breakdown of equipartition and the virial theorem. The dynamics and violation of the equipartition of the energy in the system were also probed experimentally by Afek *et al.* (2020).

Deviations from equipartition in a harmonic potential can be parametrized using the *equipartition parameter*, the square root of the ratio of the expectation value of the kinetic energy E_k to that of the potential energy E_p ,

$$\chi_H = \sqrt{\frac{E_k}{E_p}} = \sqrt{\frac{\langle p^2 \rangle}{\omega^2 \langle x^2 \rangle}}. \quad (40)$$

The relevant parameters for the description of the system are the strength of the linear friction \mathcal{A} , the momentum scale for the onset of the nonlinear friction [Eq. (6)] p_c , the diffusion constant D_0 , and the harmonic oscillation frequency of the atoms in the trap ω . All but the last parameter depend experimentally on the detuning and intensity of the Sisyphus lasers. Consider the scaled coordinates $x \rightarrow M\omega x/p_c$ and $p \rightarrow p/p_c$. There are now two dimensionless parameters that characterize the dynamics, the by now familiar \tilde{U}_0 relevant to the potential-free problem and a new parameter controlling the strength of the harmonic trap $\Omega = \omega/\mathcal{A}$. The Fokker-Planck equation is modified to a Kramers-Fokker-Planck (KFP) equation for the phase-space density, which in these scaled coordinates reads

$$\frac{\partial}{\partial t} P(x, p, t) = \left[\Omega \left(-p \frac{\partial}{\partial x} + x \frac{\partial}{\partial p} \right) + \frac{\partial}{\partial p} \left(\frac{p}{1+p^2} + \frac{1}{\tilde{U}_0} \frac{\partial}{\partial p} \right) \right] \times P(x, p, t). \quad (41)$$

The theoretical analysis focuses on the properties of the steady-state solution, which breaks down for shallow lattices such that a steady-state momentum distribution does not exist. An analysis of the time-dependent problem that is required to treat $\tilde{U}_0 < 1$ has not yet been performed.

The steady state of the KFP equation is not exactly solvable, and hence the analysis is restricted to various limits and numerics (Dechant, Kessler, and Barkai, 2015; Dechant *et al.*, 2016). In short, the numerics predict that χ_H decreases for increasing lattice depth \tilde{U}_0 , dropping to a minimum value that

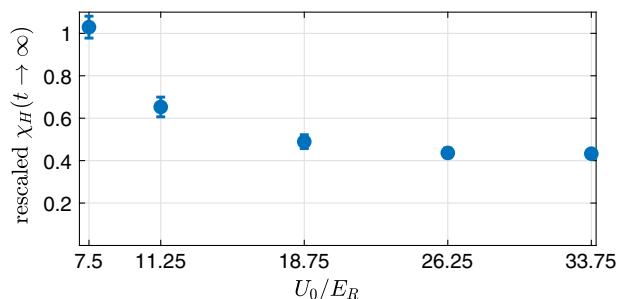


FIG. 11. Fundamental concepts such as the equipartition theorem are shown to be violated. Steady-state values of the equipartition parameter χ_H [Eq. (40)] experimentally measured for a trapped cloud of ^{87}Rb atoms (rescaled by its thermal value, which is < 1 due to trap anharmonicity), quantifying a nonmonotonic deviation from equipartition. Adapted Afek *et al.*, 2020.

depends on Ω . This is followed by an asymptotic ascent back to unity as the lattice depth increases.

Experimentally observing such a violation of equipartition requires the ability to measure $\langle x^2 \rangle$, $\langle p^2 \rangle$, and ω according to Eq. (40). Afek *et al.* (2020) used a setup similar to that described by Afek *et al.* (2017) in conjunction with a superimposed crossed-optical dipole trap providing the confining potential. The atoms were coupled to a 1D dissipative Sisyphus lattice for a given amount of time, after which their spatial and momentum distributions were imaged using direct absorption imaging and time of flight, respectively. Imaging the atomic density profile *in situ* is susceptible to imaging errors arising from the high density of the trapped atoms, and avoiding this required the researchers to homogeneously excite a controlled fraction of the atoms to the upper hyperfine state using a variable-length microwave pulse and selectively image this transferred population. This provided a knob for scanning the density of the atoms and a way of extrapolating it down to zero giving the true size of the atomic cloud in an aberration-free way. The oscillation frequency was measured independently by applying a perturbation to the trapped cloud and observing its sloshing oscillations in the trap.

The measured steady-state values of χ_H are shown in Fig. 11. They display a monotonic decrease in χ_H as the lattice depth increases, perhaps hinting at the shallow-lattice behavior numerically observed by Dechant *et al.* (2016). The work carried out by Afek *et al.* (2020) suffered greatly from the anharmonicity of the optical trapping potential. This necessitated the use of several nontrivial experimental methods to extract the harmonic χ_H .

To summarize, both theory and experiment exhibit violation of the equipartition theorem. More refined experiments and possibly an extension of the semiclassical approach are needed to quantify the effects more precisely.

V. LÉVY STATISTICS AND POWER LAWS IN OTHER ATOMIC SYSTEMS

The generality of the framework presented in this Colloquium can be appreciated by observing other atomic systems, even when instead of momentum and position one

considers a different pair of variables, for instance, phase and frequency. This has profound implications for coherence times of quantum memories. Furthermore, the question of the relation of infinite ergodic theory with other laser-cooling mechanisms is also addressed.

A. Motional broadening in two-level system ensembles with a heavy-tailed frequency distribution

Consider an oscillator whose frequency has some anomalous stochastic dynamics. This fluctuating frequency together with its time integral, namely, the phase ϕ of the oscillator, is analogous to the momentum and position whose dynamics were discussed earlier. The distribution of phases of an ensemble of oscillators spreads similarly to the spatial spreading of the particle packet, leading to decoherence, which is a limiting factor in many applications, such as atomic clocks and quantum memories based on two-level systems (Ludlow *et al.*, 2015; Heshami *et al.*, 2016). In the typical case in which the instantaneous fluctuating frequency distribution of the ensemble has finite moments, stochastic fluctuations cause the phase to spread diffusively ($\Delta\phi \sim t^{1/2}$), as compared to a ballistic spread $\Delta\phi \sim t$ for a static frequency inhomogeneity (Sagi, Almog, and Davidson, 2010). This slower diffusive spread induces the well-known effect of *motional narrowing* of the power spectrum, which also lengthens ensemble coherence times (Bloembergen, Purcell, and Pound, 1948; Romer and Dicke, 1955). When the instantaneous frequency distribution of the ensemble is heavy tailed, however, the picture is different. The stochastic phase dynamics becomes anomalous, the phase spread grows superdiffusively, and motional narrowing is hindered (Sagi *et al.*, 2011). In particular, when the first moment of the frequency distribution diverges, the stochastic frequency fluctuations can lead to *broadening* of the spectrum (motional broadening), surprisingly shortening the coherence time as the rate of fluctuations increases (Burnstein, 1981; Sagi *et al.*, 2011). For a frequency distribution following Lévy statistics $\sim \exp(-A|\kappa|^\nu)$ as in Eq. (3), the transition between motional narrowing and motional broadening occurs at $\nu = 1$, which corresponds to the Lorentzian spectrum. The coherence time of the ensemble decays as $\tau_c^{\nu-1}$ (Sagi *et al.*, 2011), with τ_c the correlation time of the fluctuating frequency. This slowing down or acceleration of the ensemble coherence decay, depending on the value of ν , is a particularly striking feature. In this respect, the fluctuations act as resetting events making motional narrowing analogous to the Zeno effect (Milburn, 1988), in which certain events, such as measurements, delay the decay of a system. By the same token, motional broadening is analogous to the anti-Zeno effect (Sagi *et al.*, 2011), where the opposite occurs.

It has been theorized (Poletti *et al.*, 2012, 2013), and recently verified experimentally (Bouganne *et al.*, 2020) with ultracold atoms in optical lattices, that strong interactions in a many-body system can also generate an anomalous decay of the coherence of the ensemble. Long-range interactions in ion chains have recently been used to probe the assumption that classical hydrodynamics can emerge universally for any complex quantum system, due to mixing of local degrees of freedom through Ising interactions with an engineered

power-law decay (Joshi *et al.*, 2022). Power-law spectral line shapes can naturally emerge in NMR due to dipolar interactions (Klauder and Anderson, 1962), long-range interactions (Holtmark, 1919), spread in activation energies (Yue, Mkhitarian, and Raikh, 2016) or hopping distances (Paladino *et al.*, 2014), and various other homogeneous imperfections (Stoneham, 1969). They are also related to ergodicity breaking in blinking quantum dots (Margolin and Barkai, 2005) and to the dynamics of photons in warm atomic vapor (Mercadier *et al.*, 2009; Baudouin *et al.*, 2014).

B. Lévy dynamics in subrecoil laser cooling

Subrecoil laser cooling (Aspect *et al.*, 1988; Kasevich and Chu, 1992) relies on a totally different mechanism than that of the sub-Doppler cooling presented in Sec. II.B, and still some of the general insights gained by analyzing one can be applied to the other, showing the generality of the toolbox presented in this Colloquium. In particular, Lévy laws are known to govern the statistical aspects of the problem, an issue previously analyzed extensively by Bardou *et al.* (2002). However, the role of infinite ergodic theory and its associated non-normalized state was only recently connected to this system (Barkai, Radons, and Akimoto, 2021). The new analysis shows that in subrecoil laser cooling there is a non-normalized state describing some of the coldest atoms that is complementary to the standard description (Bardou *et al.*, 1994).

Subrecoil laser cooling is based on carefully engineering the photon scattering rate of an atomic ensemble in such a way that slow (cold) atoms have a smaller chance of absorbing a photon from the laser than hot ones. In other words, the photon scattering rate $R(p) \rightarrow 0$ as the momentum $p \rightarrow 0$. An atom will diffuse due to random kicks from photon recoil events until its momentum becomes small enough that the scattering rate diminishes significantly, and it will linger for a lengthy period of time at low momentum and remain cold (Fig. 12). The characteristic evolution time of an atom in such a laser field is $R^{-1}(p)$, which diverges as p approaches zero. Depending on the small- p behavior of the scattering rate, the distribution of these waiting times may have heavy tails and even diverging moments, a signature of anomalous, Lévy-type dynamics.

The rate $R(p) \sim |p|^\zeta$ and ζ can be controlled experimentally (Bardou *et al.*, 1994; Reichel *et al.*, 1995; Cohen-Tannoudji and Guéry-Odelin, 2011), and one finds a non-normalized state that is controlled by the value of ζ . In particular, subrecoil laser cooling works best when the mean time the atom spends with momentum in a small interval close to zero diverges; thus, states with momentum close to the minimum of $R(p)$ plotted in Fig. 12 are extremely long lived. This means that there are long stagnation times during which the speeds are close to zero, which is the goal of cooling, but at the same time indicates the violation of the basic postulates of statistical physics.

The theoretical challenge is therefore to construct a statistical theory to replace ordinary ergodic theory based on infinite ergodic theory (Aronson, 1997; Barkai, Radons, and Akimoto, 2021). Consider the energy of the system, which in the absence of interactions is purely kinetic. For normal gases this is usually $k_B T/2$ per degree of freedom and one uses a

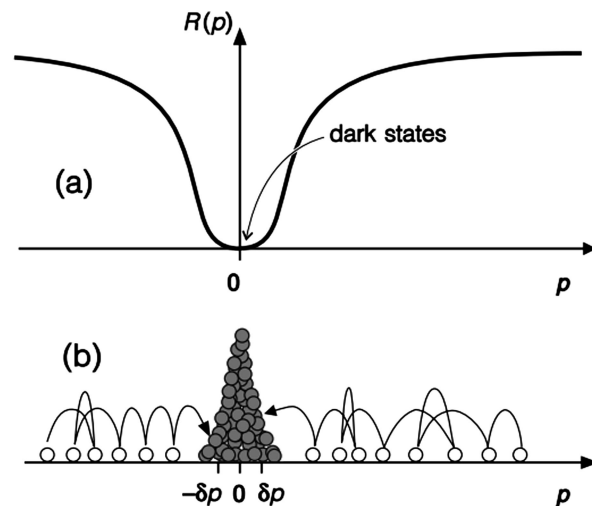


FIG. 12. Lévy statistics and power-law distributions have meaningful consequences for other atomic systems. One such system is subrecoil laser cooling. Top panel: the fluorescence rate $R(p)$ vanishes for $p \rightarrow 0$. Bottom panel: the atoms perform a random walk in momentum space and accumulate in a small interval around $p = 0$, where they remain trapped. Adapted from Bardou *et al.*, 2002.

perfectly normalized density to compute it, namely, the Maxwell-Boltzmann momentum distribution. Here one needs to use a non-normalized state with an important caveat: only when the kinetic energy is integrable with respect to the non-normalizable state is this strategy valid.

More specifically, just as for the usual ensemble averages of physical observables, which are obtained by integrating over the steady-state densities, here the non-normalized state is used, and if the result of the integration is finite the observable is classified as “integrable.” This in turn means that observables like the energy of the system go through an ergodic transition as they switch from being integrable to being nonintegrable, which is similar to the Sisyphus cooling case described by Eq. (19), where the kinetic energy is calculated from a non-normalized state only when $1 < \check{U}_0 < 3$. However, for subrecoil laser-cooled gases, the infinite density is not a description of the large momentum tail of the distribution, but rather it is relevant when the system is in the coldest state possible. This is vastly different from the Sisyphus system, and for sub-Doppler cooling the anomalous statistics is found for shallow optical lattices, and far from the ideal cooling scheme.

VI. DISCUSSION AND SUMMARY

This Colloquium highlights the unique statistical properties of atoms undergoing Sisyphus cooling. The advantage of this system is twofold: its controllability, rarely found in experimental systems exhibiting anomalous stochastic behavior, allows for a single control parameter (the depth of the optical lattice) to control the various phases of the dynamics (Fig. 10). The analysis of the scale-free process is made possible with a relatively simple tool, a Fokker-Planck equation, without invoking fractional derivatives or other *ad hoc* assumptions with regard to the power-law statistics of waiting times and

jump distances. This relates to the second striking feature of this system, which is its broad relevance. It was shown that the momentum distribution exhibits power-law statistics and a stable Lévy distribution describes the spatial spreading of the packet of particles. Though such statistics appear in many systems, physically these power laws cannot extend to infinity, as, for example, the energy of the system is always bounded.

We have shown how to employ the concept of infinite densities to describe the far tails of the corresponding densities. These non-normalized states are time-dependent solutions that match the heavy-tailed distributions and render finite otherwise infinite moments, like the energy or the mean-squared displacement. Treated for many years by mathematicians as a pure abstract theory, this infinite ergodic theory is linked here to an actual physical system. The relevance of these concepts extends beyond the cold atomic system and into the mathematical field of infinite ergodic theory, subrecoil laser cooling (Sec. V.B), properties of $1/f$ noise (Fox, Barkai, and Krapf, 2021), weak chaos, and stochastic renewal processes (Akimoto, Barkai, and Radons, 2020; Xu, Metzler, and Wang, 2022).

In addition, and extending beyond the scope of this Colloquium, the moments of the spreading particles exhibit a biscaling behavior termed strong anomalous diffusion (Castiglione *et al.*, 1999; Aghion, Kessler, and Barkai, 2017). This means that the moments of some observable $o(t)$ obey $\langle o^q \rangle \sim t^{\nu(q)}$, where $\nu(q)$ is a piecewise linear function with a single jump in slope. This behavior was experimentally observed in the context of cellular dynamics by Gal and Weihs (2010) and theorized to occur in systems such as hydrodynamics, infinite horizon Lorentz gases, and Sinai billiards.

We have seen how fundamental concepts, rooted deeply in our understanding of statistical physics, are violated in this system. Among them was the Einstein-Green-Kubo formalism (typically relating the diffusivity to a stationary correlation function), which needed to be replaced with one that takes into account the aging of the correlation function in this system. This results in the ability to calculate transport constants previously predicted to be infinite. This aging of the correlation function is generally related to the $1/f$ noise spectrum [for example, in the context of protein diffusion on the cell membrane (Fox, Barkai, and Krapf, 2021)], as well as to glassy systems, where magnetization correlation functions exhibit similar aging (Bouchaud, 1992). Other fundamental implications reviewed were deviations from the Boltzmann-Gibbs equilibrium state and the equipartition theorem, as well as the application of infinite ergodic theory to an exploration of the breakdown of ergodicity.

Looking forward to the missing pieces of the puzzle, another laser-cooling scheme emerges as both a theoretical and an experimental candidate for anomalous dynamics—that of Raman-sideband cooling (Vuletić *et al.*, 1998; Kerman *et al.*, 2000; Hu *et al.*, 2017; Zohar *et al.*, 2022). In this scheme, atoms are trapped in the potential wells of a far-detuned standing wave. The trapping beams induce Raman transitions and remove vibrational quanta, cooling the trapped atoms to the lowest vibrational state. Optical pumping needed

to close the cooling cycle involves spontaneous Raman scattering that may change the vibrational state, and thus heat the atoms. For low vibrational states, such heating is minimized by the Lamb-Dicke effect (Vuletić *et al.*, 1998), thereby yielding efficient cooling. However, at high vibrational states optical pumping results in excessive heating where nonstandard statistics may become plausible. As it is typically preceded by precooling into the Lamb-Dicke regime by other cooling methods, such anomalous statistics have not been observed thus far. Equipartition violations in transient states have been observed and even used in the context of this scheme to optimize the cooling (Hu *et al.*, 2017; Mayer *et al.*, 2020).

Another relevant aspect may be the effects of many-body physics on the anomalous statistics. How will atom-atom interactions drive the system to thermal equilibrium? Will this depend on the depth of the optical lattice, and if so, how? Another unexplored aspect of the problem relates to the Green-Kubo formalism. In transport theory, the relation between the responses to a linear external weak field, namely, the calculation of the mobility of the system, is a standard problem. Further exploration into this issue could serve a wider audience interested in anomalous response functions.

The study of the dynamics of the relaxation of the system to its steady state, explored theoretically by Hirschberg, Mukamel, and Schütz (2011, 2012), requires temporal control over the lattice parameters, a feature inherently available in ultracold atomic experiments. By “quenching” the power of the lattice lasers from different initial conditions to different final states, one can explore how the system approaches the steady state (Afek, 2019). An ac temporal modulation of the lattice depth was performed by Wickenbrock *et al.* (2012). This renormalizes \tilde{U}_0 and may allow access to an effective shallow-lattice regime, thus revealing the elusive Richardson phase of Eq. (23) (Barkai, Aghion, and Kessler, 2014).

Furthermore, one can consider two new experimental frontiers: the first statistics focused and the second single-particle focused, each with its own advantages. The former is rooted in the fact that rare events and heavy tails require many decades of signal to noise to be resolved properly, whereas the latter is appealing in the sense that direct observations of trajectories can yield insights into the underlying processes that are washed out in the measurements of a large ensemble of particles. In particular, with single-particle trajectories one can in principle analyze the time averages computed from long trajectories and see how they are related to ensemble averages. This will promote a better understanding of the ergodic hypothesis in systems with scale-free dynamics. Modification of the external confining potential is also expected to lead to intricate behaviors that have yet to be fully explored. A third, crossover regime is now slowly being made accessible through recent advances in the trapping of large arrays of single atoms (Morgado and Whitlock, 2021) and ions (Joshi *et al.*, 2022) combining single-particle control with relatively large statistics.

ACKNOWLEDGMENTS

The authors thank Erez Aghion and Ariel Amir for their valuable input on the manuscript, and Erez Aghion, Andreas

Dechant, Eric Lutz, and Yoav Sagi for important contributions to the work discussed in this Colloquium. D. A. K. and E. B. acknowledge the support of Israel Science Foundation Grant No. 1614/21.

REFERENCES

- Aaronson, J., 1997, *An Introduction to Infinite Ergodic Theory* (American Mathematical Society, Providence), p. 50.
- Afek, G., 2019, “Anomalous phase-space dynamics of cold atoms,” Ph.D. thesis (Weizmann Institute of Science).
- Afek, G., A. Cheplov, A. Courvoisier, and N. Davidson, 2020, *Phys. Rev. A* **101**, 042123.
- Afek, G., J. Coslovsky, A. Courvoisier, O. Livneh, and N. Davidson, 2017, *Phys. Rev. Lett.* **119**, 060602.
- Agarwal, G., and K. Molmer, 1993, *Phys. Rev. A* **47**, 5158.
- Aghion, E., D. A. Kessler, and E. Barkai, 2017, *Phys. Rev. Lett.* **118**, 260601.
- Aghion, E., D. A. Kessler, and E. Barkai, 2019, *Phys. Rev. Lett.* **122**, 010601.
- Agranov, T., P. Zilber, N. R. Smith, T. Admon, Y. Roichman, and B. Meerson, 2020, *Phys. Rev. Res.* **2**, 013174.
- Akimoto, T., 2008, *J. Stat. Phys.* **132**, 171.
- Akimoto, T., E. Barkai, and G. Radons, 2020, *Phys. Rev. E* **101**, 052112.
- Albers, T., and G. Radons, 2018, *Phys. Rev. Lett.* **120**, 104501.
- Alt, W., D. Schrader, S. Kuhr, M. Müller, V. Gomer, and D. Meschede, 2003, *Phys. Rev. A* **67**, 033403.
- Amir, A., 2020, *Thinking Probabilistically: Stochastic Processes, Disordered System, and Their Applications* (Cambridge University Press, Cambridge, England).
- Anderson, M., J. Ensher, M. Matthews, C. Wieman, and E. Cornell, 1995, *Science* **269**, 198.
- Ariel, G., A. Rabani, S. Benisty, J. D. Partridge, R. M. Harshey, and A. Be’er, 2015, *Nat. Commun.* **6**, 8396.
- Aspect, A., E. Arimondo, R. Kaiser, N. Vansteenkiste, and C. Cohen-Tannoudji, 1988, *Phys. Rev. Lett.* **61**, 826.
- Bar, A., Y. Kafri, and D. Mukamel, 2007, *Phys. Rev. Lett.* **98**, 038103.
- Bar, A., Y. Kafri, and D. Mukamel, 2009, *J. Phys. Condens. Matter* **21**, 034110.
- Bardou, F., J.-P. Bouchaud, A. Aspect, and C. Cohen-Tannoudji, 2002, *Lévy Statistics and Laser Cooling: How Rare Events Bring Atoms to Rest* (Cambridge University Press, Cambridge, England).
- Bardou, F., J.-P. Bouchaud, O. Emile, A. Aspect, and C. Cohen-Tannoudji, 1994, *Phys. Rev. Lett.* **72**, 203.
- Barkai, E., E. Aghion, and D. Kessler, 2014, *Phys. Rev. X* **4**, 021036.
- Barkai, E., A. Naumov, Y. Vainer, M. Bauer, and L. Kador, 2003, *Phys. Rev. Lett.* **91**, 075502.
- Barkai, E., G. Radons, and T. Akimoto, 2021, *Phys. Rev. Lett.* **127**, 140605.
- Barkai, E., R. Silbey, and G. Zumofen, 2000, *Phys. Rev. Lett.* **84**, 5339.
- Baudouin, Q., R. Pierrat, A. Eloy, E. J. Nunes-Pereira, P.-A. Cuniasse, N. Mercadier, and R. Kaiser, 2014, *Phys. Rev. E* **90**, 052114.
- Bloembergen, N., E. Purcell, and R. Pound, 1948, *Phys. Rev.* **73**, 679.
- Bothe, M., F. Sagues, and I. Sokolov, 2019, *Phys. Rev. E* **100**, 012117.
- Bouchaud, J.-P., 1992, *J. Phys. I (France)* **2**, 1705.
- Bouchaud, J.-P., and A. Georges, 1990, *Phys. Rep.* **195**, 127.
- Bouganne, R., M. B. Aquilera, A. Ghermaoui, J. Beugnon, and F. Gerbier, 2020, *Nat. Phys.* **16**, 21.
- Bray, A., 2000, *Phys. Rev. E* **62**, 103.
- Brokman, X., J. Hermier, G. Messin, P. Desbiolles, J.-P. Bouchaud, and M. Dahan, 2003, *Phys. Rev. Lett.* **90**, 120601.
- Burnstein, A., 1981, *Chem. Phys. Lett.* **83**, 335.
- Burov, S., R. Metzler, and E. Barkai, 2010, *Proc. Natl. Acad. Sci. U.S.A.* **107**, 13228.
- Castiglione, P., A. Mazzino, P. Muratore-Ginanneschi, and A. Vulpiani, 1999, *Physica (Amsterdam)* **134D**, 75.
- Castin, Y., J. Dalibard, and C. Cohen-Tannoudji, 1991, in *Light Induced Kinetic Effects on Atoms, Ions, and Molecules*, edited by L. Moi, S. Gozzini, C. Gabbanini, E. Arimondo, and F. Strumia (Edizioni ETS, Pisa), p. 5.
- Castin, Y., and K. Molmer, 1990, *J. Phys. B* **23**, 4101.
- Chandrasekhar, S., 1943, *Rev. Mod. Phys.* **15**, 1.
- Chistyakov, V., 1964, *Theory Probab. Appl.* **9**, 640.
- Chu, S., 1998, *Rev. Mod. Phys.* **70**, 685.
- Cohen-Tannoudji, C., 1998, *Rev. Mod. Phys.* **70**, 707.
- Cohen-Tannoudji, C., and D. Guéry-Odelin, 2011, *Advances in Atomic Physics: An Overview* (World Scientific, Singapore).
- Dalibard, J., and C. Cohen-Tannoudji, 1989, *J. Opt. Soc. Am. B* **6**, 2023.
- Darling, D. A., and M. Kac, 1957, *Trans. Am. Math. Soc.* **84**, 444.
- Dechant, A., D. A. Kessler, and E. Barkai, 2015, *Phys. Rev. Lett.* **115**, 173006.
- Dechant, A., F. Kindermann, A. Widera, and E. Lutz, 2019, *Phys. Rev. Lett.* **123**, 070602.
- Dechant, A., E. Lutz, E. Barkai, and D. Kessler, 2011, *J. Stat. Phys.* **145**, 1524.
- Dechant, A., E. Lutz, D. Kessler, and E. Barkai, 2011, *Phys. Rev. Lett.* **107**, 240603.
- Dechant, A., E. Lutz, D. Kessler, and E. Barkai, 2012, *Phys. Rev. E* **85**, 051124.
- Dechant, A., E. Lutz, D. Kessler, and E. Barkai, 2014, *Phys. Rev. X* **4**, 011022.
- Dechant, A., S. T. Shafier, D. A. Kessler, and E. Barkai, 2016, *Phys. Rev. E* **94**, 022151.
- Dion, C. M., S. Jonsell, A. Kastberg, and P. Sjölund, 2016, *Phys. Rev. A* **93**, 053416.
- Douglas, P., S. Bergamini, and F. Renzoni, 2006, *Phys. Rev. Lett.* **96**, 110601.
- Duplat, J., S. Kheifets, T. Li, M. Raizen, and E. Villermanx, 2013, *Phys. Rev. E* **87**, 020105.
- Falasco, G., E. Barkai, and M. Baiesi, 2022, *Phys. Rev. E* **105**, 024143.
- Fogedby, H. C., and R. Metzler, 2007a, *Phys. Rev. Lett.* **98**, 070601.
- Fogedby, H. C., and R. Metzler, 2007b, *Phys. Rev. E* **76**, 061915.
- Foot, C. J., 2005, *Atomic Physics*, Vol. 7 (Oxford University Press, New York).
- Fox, Z. R., E. Barkai, and D. Krapf, 2021, *Nat. Commun.* **12**, 6162.
- Gal, N., and D. Weihs, 2010, *Phys. Rev. E* **81**, 020903.
- Gardiner, C., 1985, *Handbook of Stochastic Methods*, Vol. 3 (Springer, Berlin).
- Gaunt, A. L., T. F. Schmidutz, I. Gotlibovych, R. P. Smith, and Z. Hadzibabic, 2013, *Phys. Rev. Lett.* **110**, 200406.
- Gillespie, D. T., and E. Seitaridou, 2012, *Simple Brownian Diffusion: An Introduction to the Standard Theoretical Models* (Oxford University Press, New York).
- Godreche, C., and J. Luck, 2001, *J. Stat. Phys.* **104**, 489.
- Green, M. S., 1954, *J. Chem. Phys.* **22**, 398.
- Hanke, A., and R. Metzler, 2003, *J. Phys. A* **36**, L473.
- Hänsch, T., and A. Schawlow, 1975, *Opt. Commun.* **13**, 68.

- Heshami, K., D. G. England, P. C. Humphreys, P. J. Bustard, V. M. Acosta, J. Nunn, and B. J. Sussman, 2016, *J. Mod. Opt.* **63**, 2005.
- Hirschberg, O., D. Mukamel, and G. M. Schütz, 2011, *Phys. Rev. E* **84**, 041111.
- Hirschberg, O., D. Mukamel, and G. M. Schütz, 2012, *J. Stat. Mech.* P02001.
- Hnggi, P., and F. Marchesoni, 2005, *Chaos* **15**, 026101.
- Hodapp, T., C. Gerz, C. Furtlehner, C. Westbrook, W. D. Phillips, and J. Dalibard, 1995, *Appl. Phys. B* **60**, 135.
- Holtmark, J., 1919, *Ann. Phys. (Berlin)* **363**, 577.
- Holz, P. C., A. Dechant, and E. Lutz, 2015, *Europhys. Lett.* **109**, 23001.
- Hu, J., A. Urvoy, Z. Vendeiro, V. Crpel, W. Chen, and V. Vuletić, 2017, *Science* **358**, 1078.
- Jersblad, J., H. Ellmann, and A. Kastberg, 2000, *Phys. Rev. A* **62**, 051401.
- Jersblad, J., H. Ellmann, K. Stöckel, A. Kastberg, L. Sanchez-Palencia, and R. Kaiser, 2004, *Phys. Rev. A* **69**, 013410.
- Joshi, M. K., F. Kranzl, A. Schuckert, I. Lovas, C. Maier, R. Blatt, M. Knap, and C. F. Roos, 2022, *Science* **376**, 720.
- Kanazawa, K., T. Sano, A. Cairoli, and A. Baule, 2020, *Nature (London)* **579**, 364.
- Kasevich, M., and S. Chu, 1992, *Phys. Rev. Lett.* **69**, 1741.
- Kasevich, M., D. S. Weiss, E. Riis, K. Moler, S. Kasapi, and S. Chu, 1991, *Phys. Rev. Lett.* **66**, 2297.
- Katori, H., S. Schlipf, and H. Walther, 1997, *Phys. Rev. Lett.* **79**, 2221.
- Kelly, J. F., and M. M. Meerschaert, 2019, in *Handbook of Fractional Calculus with Applications*, Vol. 5, Applications in Physics Part B, edited by V. E. Tarasov (De Gruyter, Berlin), pp. 129–150.
- Kerman, A. J., V. Vuletić, C. Chin, and S. Chu, 2000, *Phys. Rev. Lett.* **84**, 439.
- Kessler, D. A., and E. Barkai, 2010, *Phys. Rev. Lett.* **105**, 120602.
- Kessler, D. A., and E. Barkai, 2012, *Phys. Rev. Lett.* **108**, 230602.
- Kindermann, F., A. Dechant, M. Hohmann, T. Lausch, D. Mayer, F. Schmidt, E. Lutz, and A. Widera, 2017, *Nat. Phys.* **13**, 137.
- Klauder, J., and P. Anderson, 1962, *Phys. Rev.* **125**, 912.
- Korabel, N., and E. Barkai, 2009, *Phys. Rev. Lett.* **102**, 050601.
- Kostylev, N., E. Ivanov, M. E. Tobar, and J. J. McFerran, 2014, *J. Opt. Soc. Am. B* **31**, 1614.
- Kubo, R., 1957, *J. Phys. Soc. Jpn.* **12**, 570.
- Landau, L. D., 1944, *J. Phys. (USSR)* **8**, 201.
- Letokhov, V., and V. Minogin, 1981, *Phys. Rep.* **73**, 1.
- Levine, E., D. Mukamel, and G. M. Schütz, 2005, *Europhys. Lett.* **70**, 565.
- Lévy, P., 1937, *Monographies des Probabilités*, Vol. 1 (Gauthier-Villars, Paris).
- Livneh, O., G. Afek, and N. Davidson, 2018, *Appl. Opt.* **57**, 3205.
- Ludlow, A. D., M. M. Boyd, J. Ye, E. Peik, and P. O. Schmidt, 2015, *Rev. Mod. Phys.* **87**, 637.
- Lutz, E., 2003, *Phys. Rev. A* **67**, 051402.
- Lutz, E., 2004, *Phys. Rev. Lett.* **93**, 190602.
- Lutz, E., and F. Renzoni, 2013, *Nat. Phys.* **9**, 615.
- Majumdar, S., 2007, in *The Legacy of Albert Einstein: A Collection of Essays in Celebration of the Year of Physics* (World Scientific, Singapore), pp. 93–129.
- Majumdar, S. N., and A. Comtet, 2004, *Phys. Rev. Lett.* **92**, 225501.
- Majumdar, S. N., and A. Comtet, 2005, *J. Stat. Phys.* **119**, 777.
- Mandelbrot, B. B., 1982, *The Fractal Geometry of Nature*, Vol. 1 (W. H. Freeman, New York).
- Manning, G. S., 1969, *J. Chem. Phys.* **51**, 924.
- Mantegna, R. N., and H. E. Stanley, 1999, *Introduction to Econophysics: Correlations and Complexity in Finance* (Cambridge University Press, Cambridge, England).
- Margolin, G., and E. Barkai, 2004, *J. Chem. Phys.* **121**, 1566.
- Margolin, G., and E. Barkai, 2005, *Phys. Rev. Lett.* **94**, 080601.
- Margolin, G., V. Protasenko, M. Kuno, and E. Barkai, 2006, *J. Phys. Chem. B* **110**, 19053.
- Marksteiner, S., K. Ellinger, and P. Zoller, 1996, *Phys. Rev. A* **53**, 3409.
- Martin, E., U. Behn, and G. Germano, 2011, *Phys. Rev. E* **83**, 051115.
- Mayer, D., F. Schmidt, S. Haupt, Q. Bouton, D. Adam, T. Lausch, E. Lutz, and A. Widera, 2020, *Phys. Rev. Res.* **2**, 023245.
- Meir, Z., T. Sikorsky, R. Ben-shlomi, N. Akerman, Y. Dallal, and R. Ozeri, 2016, *Phys. Rev. Lett.* **117**, 243401.
- Mercadier, N., W. Guerin, M. Chevrollier, and R. Kaiser, 2009, *Nat. Phys.* **5**, 602.
- Metzler, R., J.-H. Jeon, A. G. Cherstvy, and E. Barkai, 2014, *Phys. Chem. Chem. Phys.* **16**, 24128.
- Metzler, R., and J. Klafter, 2000, *Phys. Rep.* **339**, 1.
- Miccichè, S., 2010, *Europhys. Lett.* **92**, 50011.
- Milburn, G. J., 1988, *J. Opt. Soc. Am. B* **5**, 1317.
- Moler, K., D. S. Weiss, M. Kasevich, and S. Chu, 1992, *Phys. Rev. A* **45**, 342.
- Montroll, E. W., and G. H. Weiss, 1965, *J. Math. Phys. (N.Y.)* **6**, 167.
- Morgado, M., and S. Whitlock, 2021, *AVS Quantum Sci.* **3**, 023501.
- Navon, N., R. P. Smith, and Z. Hadzibabic, 2021, *Nat. Phys.* **17**, 1334.
- Nienenzu, W., T. Grießer, and H. Ritsch, 2011, *Europhys. Lett.* **96**, 43001.
- Paladino, E., Y. M. Galperin, G. Falci, and B. L. Altshuler, 2014, *Rev. Mod. Phys.* **86**, 361.
- Phillips, W. D., 1998, *Rev. Mod. Phys.* **70**, 721.
- Poland, D., and H. A. Scheraga, 1966, *J. Chem. Phys.* **45**, 1456.
- Poletti, D., P. Barmettler, A. Georges, and C. Kollath, 2013, *Phys. Rev. Lett.* **111**, 195301.
- Poletti, D., J.-S. Bernier, A. Georges, and C. Kollath, 2012, *Phys. Rev. Lett.* **109**, 045302.
- Ray, S., and S. Reuveni, 2020, *J. Chem. Phys.* **152**, 234110.
- Redner, S., 2001, *A Guide to First-Passage Processes* (Cambridge University Press, Cambridge, England).
- Reichel, J., F. Bardou, M. B. Dahan, E. Peik, S. Rand, C. Salomon, and C. Cohen-Tannoudji, 1995, *Phys. Rev. Lett.* **75**, 4575.
- Richardson, L., 1926, *Proc. R. Soc. A* **110**, 709.
- Romer, R., and R. Dicke, 1955, *Phys. Rev.* **99**, 532.
- Sagi, Y., I. Almog, and N. Davidson, 2010, *Phys. Rev. Lett.* **105**, 093001.
- Sagi, Y., M. Brook, I. Almog, and N. Davidson, 2012, *Phys. Rev. Lett.* **108**, 093002.
- Sagi, Y., R. Pugatch, I. Almog, N. Davidson, and M. Aizenman, 2011, *Phys. Rev. A* **83**, 043821.
- Saubaméa, B., T. W. Hijmans, S. Kulin, E. Rasel, E. Peik, M. Leduc, and C. Cohen-Tannoudji, 1997, *Phys. Rev. Lett.* **79**, 3146.
- Saubaméa, B., M. Leduc, and C. Cohen-Tannoudji, 1999, *Phys. Rev. Lett.* **83**, 3796.
- Scher, H., and E. W. Montroll, 1975, *Phys. Rev. B* **12**, 2455.
- Shlesinger, M. F., B. J. West, and J. Klafter, 1987, *Phys. Rev. Lett.* **58**, 1100.
- Shlesinger, M. F., G. M. Zaslavsky, and U. Frisch, 1995, *Lévy Flights and Related Topics in Physics* (Springer, New York).
- Shusterman, R., S. Alon, T. Gavrinov, and O. Krichevsky, 2004, *Phys. Rev. Lett.* **92**, 048303.
- Sokolov, I. M., and J. Klafter, 2005, *Chaos* **15**, 026103.

- Song, M. S., H. C. Moon, J.-H. Jeon, and H. Y. Park, 2018, *Nat. Commun.* **9**, 1.
- Stefani, F. D., J. Hoogenboom, and E. Barkai, 2009, *Phys. Today* **62**, No. 2, 34.
- Stigler, S. M., 1986, *The History of Statistics: The Measurement of Uncertainty before 1900* (Harvard University Press, Cambridge, MA).
- Stoneham, A., 1969, *Rev. Mod. Phys.* **41**, 82.
- Taylor, G. I., 1922, *Proc. London Math. Soc.* **s2-20**, 196.
- Tuchendler, C., A. M. Lance, A. Browaeys, Y. R. P. Sortais, and P. Grangier, 2008, *Phys. Rev. A* **78**, 033425.
- Van Kampen, N. G., 2007, *Stochastic Processes in Chemistry and Physics* (North-Holland, Amsterdam).
- Vezzani, A., E. Barkai, and R. Burioni, 2019, *Phys. Rev. E* **100**, 012108.
- Vezzani, A., E. Barkai, and R. Burioni, 2020, *Sci. Rep.* **10**, 1.
- Vuletić, V., C. Chin, A. Kerman, and S. Chu, 1998, *Phys. Rev. Lett.* **81**, 5768.
- Wickenbrock, A., P. C. Holz, N. A. A. Wahab, P. Phoonthong, D. Cubero, and F. Renzoni, 2012, *Phys. Rev. Lett.* **108**, 020603.
- Wineland, D. J., and H. Dehmelt, 1975, *Bull. Am. Phys. Soc.* **20**, 637.
- Wineland, D. J., R. E. Drullinger, and F. L. Walls, 1978, *Phys. Rev. Lett.* **40**, 1639.
- Xu, P., R. Metzler, and W. Wang, 2022, *Phys. Rev. E* **105**, 044118.
- Yue, Z., V. V. Mkhitaryan, and M. E. Raikh, 2016, *Phys. Rev. B* **93**, 195319.
- Zaburdaev, V., S. Denisov, and J. Klafter, 2015, *Rev. Mod. Phys.* **87**, 483.
- Zheng, W., and N. R. Cooper, 2018, *Phys. Rev. A* **97**, 021601.
- Zohar, E., Y. Florschaim, O. Zilberman, A. Stern, and Y. Sagi, 2022, *Phys. Rev. A* **106**, 063111.